Constraints on the Presence or Absence of Post-Perovskite in the Lowermost Mantle from Long-Period Seismology

Christine Houser*

Department and Earth and Planetary Sciences, University of California Santa Cruz

In this study, the ability to detect post-perovskite is examined using three long-period seismology approaches; normal modes, arrival time variations, and seismic tomography. Although normal modes provide robust integral constraints on 1D velocity and density profiles of the Earth, their ability to resolve variations in shear velocity and density decreases near the core-mantle boundary (CMB). Therefore, it is possible for post-perovskite to exist globally within 200 km of the CMB without resolution by normal modes. Deep-turning long-period *S* wave arrival times are examined in regions of dense ray coverage and a shift representing an increase in velocity consistent with presence of post-perovskite is observed in localized areas approximately 100 km above the CMB. Therefore, post-perovskite is not a ubiquitous feature but may be locally stable within both tomographically slow and fast regions near the CMB. To globally determine if regions are cold or iron-enriched enough for post-perovskite to be stable, recent thermo-chemical models are applied to a suite of geotherms and phase transition depths. The results suggest that variations in iron content are too small to control the stability of post-perovskite. It is demonstrated that only a narrow range of temperatures and phase transition depths can allow post-perovskite to exist in anomalously fast (cold) regions in the lowermost mantle. Furthermore, if post-perovskite is a major constituent of fast regions, then the temperature at 2780 km depth ranges from 2400 K – 2700 K, and post-peorvskite does not explain the observed anti-correlation of shear velocity and bulk sound speed near the CMB.

1. INTRODUCTION

The initial observations that perovskite transforms to what is now known as the post-perovskite phase [*Oganov and Ono,* 2004; *Murakami et al.,* 2004; *Tsuchiya et al.,* 2004a,b] have invigorated not only mineral physics, but also the fields of seismology and the dynamics of the deep Earth. First principles calculations find that the post-perovskite phase has a 1-1.5% increase in density, 2-4% increase in shear velocity, and ±0.5% change in compressional velocity compared to perovskite [*Tsuchiya et al.,* 2004a,b; *Oganov and Ono,* 2004; *Stackhouse et al.,* 2005a; *Wentzcovich, et al*., 2006]. These studies indicate that there are two major elastic differences between perovskite (Pv) and post-perovskite (pPv). The first is that the transformation of Pv to pPv results in an increase in shear modulus that is much larger than the increase in bulk modulus. Thus, the calculated change in shear velocity from Pv to pPv is larger than the calculated change in compressional velocity. For some time, short-period seismology has revealed areas within D″ (the lowermost 300 km of the mantle, *Bullen* [1949]) exhibiting strong reflections of shear energy, but not as much in

*Formerly Christine Reif

[book title–to come]
Geophysical Monograph Series XXX

XX.XXXX/XXXGM0X

compressional energy [*Wysession et al*., 1998]. Therefore, the transition to post-perovskite provides an attractive explanation for these reflective regions and is thoroughly discussed by *Lay and Garnero* [this volume]. The second major difference is that the layered structure of post-perovskite suggests that, if textured as a result of deformation, it is capable of being highly anisotropic. The implications of post-perovskite anisotropy are explored in detail by *Wookey and Kendall* [this volume]. Dynamic calculations are currently incorporating the effects of the properties of the Pv to pPv phase change [*Nakagawa and Tackley,* 2006; *Tackley et al.*, this volume] to test the feasibility and implications of maintaining post-perovskite throughout Earth's history. This study contributes to the dialog concerning the Pv to pPv transition by focusing on the how the occurrence of post-perovskite in the lowermost mantle is constrained globally by long-period seismology.

Long-period seismology is a powerful tool for revealing the large-scale properties of the Earth's interior. Observations of very long periods of vibration, known as normal modes, provide a means to accurately determine the 1D velocity and density profile of the Earth [*Dziewonski and Anderson,* 1981]. Arrival times of long-period seismic waves are used to map out 3D velocity structure of the mantle through seismic tomography [*Grand*, 1994; *Masters et al.,* 2000; *Gu et al.,* 2001; *Ritsema and van Heijst,* 2002; *Antolik et al.,* 2003; *Montelli et al.,* 2004; *Simmons et al.,* 2006; *Houser et al.,* 2007]. Waveform modeling is also used as a basis for seismic tomography [*Woodhouse and Dziewonski,* 1984; *Dziewonski and Woodhouse,* 1987; *Tanimoto,* 1990; *Su and Dziewonski,* 1991; *Li and Romanowicz,* 1995*; Megnin and Romanowicz,* 2000; *Panning and Romanowicz,* 2006], but is not implemented here. While normal modes are most useful for 1D structure, observations of mode splitting can be applied to seismic tomography to uncover velocity and density anomalies at very long wavelengths [*Giardini et al.,* 1987; *He and Tromp,* 1996; *Masters et al.*, 2000; *Ishii and Tromp,* 2001, 2004; *Beghein et al.,* 2002]. The general structure of the Earth's interior from these various tomographic models is surprisingly consistent despite differences in the data and the inversion methods [*Romanowicz,* 2003]. Thus, long-period seismology has provided the dynamics, mineral physics, and geochemistry communities a basis with which to evaluate potential Earth models. Despite its ability to provide direct observations of the majority of the Earth's interior, long-period seismology has not yet been applied to constrain the presence or absence of post-perovskite in the lowermost mantle.

Since the Earth's background microseism noise level peaks at roughly 7 and 14 seconds, instruments were historically designed to record data at long-periods (above 14 seconds) and short-periods (below 7 seconds). With the availability of broadband stations, the designation of long and short period arises mainly from how the seismograms are filtered, although there are many short-period networks that do not have the bandwidth to make long-period recordings. The advantages of long-period data include that they occur in a noise low, have simple pulse shapes, and subsequent *P* and *S* phases are not drowned out in the coda of the initial *P* and *S* arrivals. However, unlike short-period seismograms, in which the onset of a phase is often sharply and unambiguously defined, long-period data have broad pulse shapes making it difficult to consistently determine the onset of a phase. Therefore, long-period phases must be compared to similar long-period phases to measure their relative time shifts [*Woodward and Masters,* 1991a,b; *Grand*, 1994; *Bolton and Masters,* 2001; *Ritsema and van Heijst,* 2002; *Houser et al.,* 2007].

Early long-period networks include the Worldwide Standardized Seismographic Network (WWSSN), the Seismic Research Observatory (SRO), the United States National Seismic Network (USNSN), and the International Deployment of Accelerometers (IDA). Over time, other networks developed and expanded in the United States and other countries until their consolidation into the Incorporated Research Institutions for Seismology (IRIS) in the late 1980s. The instruments used in the early networks were designed with a dominant period around 20 seconds, so studies that use these early data will thus filter the more recent recordings to match the frequency content of the early stations. The observed seismic phases in these long-period traces are sensitive to structures with wavelengths of about 200 km. However, the parameterizations used in global long-period seismic tomography studies are usually much coarser. The shear and compressional models HMSL –S06 and HMSL – P06 from *Houser et al.* [2007] have 4° block spacing with 100 km thick blocks in the upper mantle and 200 km thick blocks in the lower mantle, and are among the finest-scale parameterizations that are available to date.

Despite the emphasis often placed on the theory and parameterization of tomographic models [*Li and Romanowicz,* 1995; *Montelli et al.,* 2004], the most important factor in any long or short-period study is the data coverage. Plate 1 shows the distribution of *S* rays turning at a distance range of 90° - 100°, which corresponds approximately to depths of 2600 km down to the core-mantle boundary for the entire IRIS long-period database from 1976 through 2005. The coverage is concentrated under eastern Eurasia and the central northern Pacific along with smaller regions under the Cocos plate, the mid-northern Atlantic, and north of Papua New Guinea. While some of these regions in the central Pacific are sampled by thousands of rays, some regions remain untouched. Plate 1 is based on all the available data and does not take into account the quality of the data. While there are over 100,000 traces represented in Plate 1, only about 14,000 of

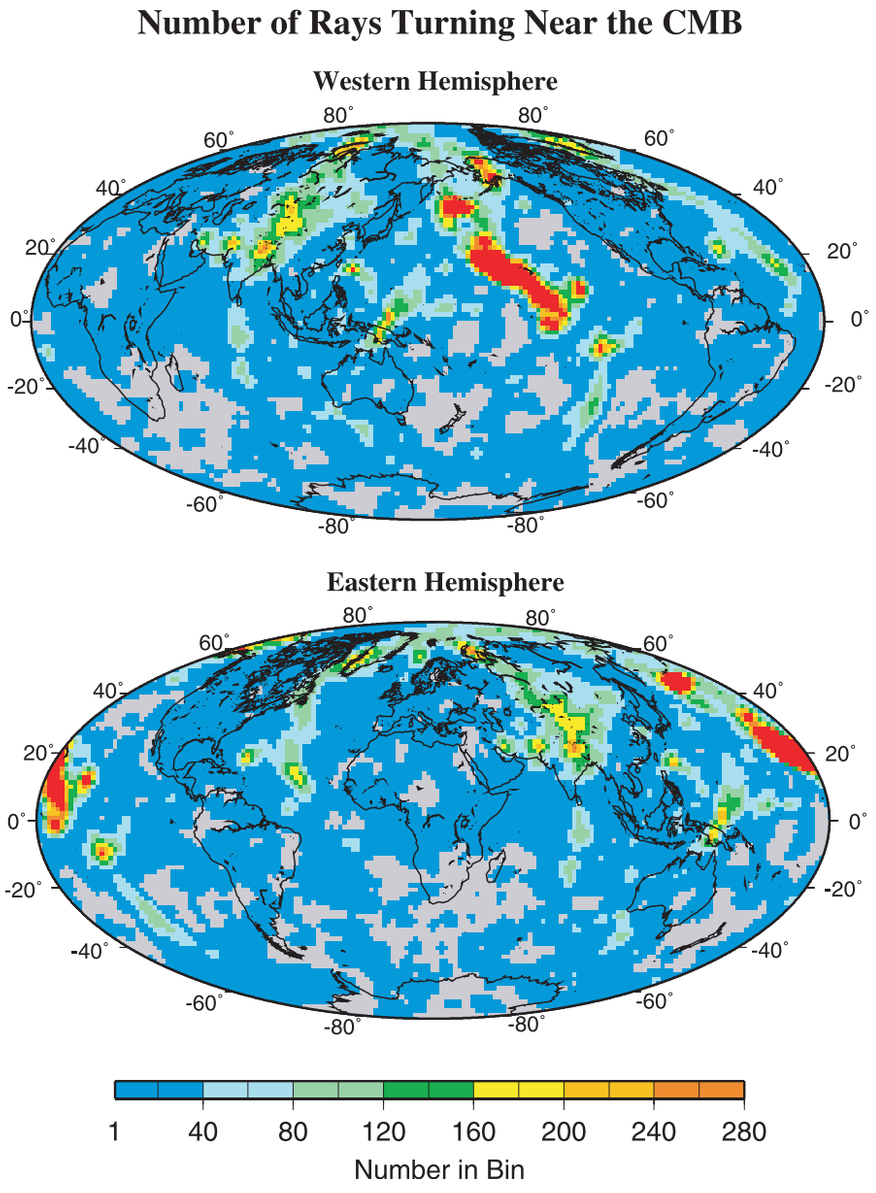

Plate 1. Western and Eastern Hemisphere views of the number of direct *S* rays in the IRIS long-period database turning at distances between 90° and 100° within 4° diameter bins. Grey regions indicate areas with no turning rays in this distance range. Red regions indicate that the number of turning rays exceeds 240. The best coverage is in the central Pacific where the number of rays often exceeds 1000.

those data, or 14%, pass the quality control criteria of *Houser et al.* [2007], and this subset is used in defining Earth structure. The two most common reasons traces are excluded from processing is that either their signal to noise ratio is too low or there is a glitch in the recording. Thus, Plate 1 demonstrates how data availability is the biggest obstacle to understanding the processes that occur near the core-mantle boundary (CMB).

For a more global analysis, long-period seismology is aided by the addition of phases other than direct *S* or *P*. Long-period phase arrivals can be inspected for the global distribution of fast and slow time residuals as well as patterns in the travel times with depth [*Bolton and Masters,* 2001]. However, the most common application is the collection of long-period travel times for mantle tomography. The core-reflected phase *ScS*, which arrives at shorter distances of 40° - 70°, greatly improves CMB coverage. Short period studies of precursors to *ScS* arrivals are confined to well-sampled regions as they rely on stacking seismic records [*Russell et al.,* 1999; *Avants et al.,* 2006]. However, measuring the long-period arrival times of these phases provides constraints on the longer-wavelength features near the CMB. In fact, the combination of direct *S* and *ScS-S* provides almost global coverage at the CMB, such that tomography models which incorporate these two phases (as well as any additional phases such as *SKS* or S_{diff}) are reasonably resolved. Since the liquid outer core does not transmit shear energy, *S* waves reflect off the boundary as if it were a free surface. However, *P* waves do not have as high an impedance contrast across the boundary, making *PcP* a low amplitude phase that is not observed in individual seismograms. Therefore, the *P* coverage at the CMB is mostly confined to the zones indicated in Plate 1, except when additional phases such as *PKP* or P_{diff} are used. Consequently, we have a better understanding of the shear velocity structure than the compressional velocity structure near the CMB. Due to the greater reliability of shear velocity structure and the greater change in shear velocities from Pv to pPv, this study concentrates on the analysis of *S* waveforms and shear velocity models.

There are essentially three possibilities for the existence of post-perovskite. 1) Post-perovskite is a global feature of the lowermost mantle. 2) Post-perovskite does not exist in the lowermost mantle. 3) The presence of post-perovskite varies laterally at long or short scales in the lowermost mantle. Here, a series of hypothesis tests are performed to investigate these possibilities and converge on a range of physical parameters for which post-perovskite could exist and explain observations of long-period data. First, the probability that post perovskite exists as a ubiquitous layer is analyzed using normal modes. Next, the predicted effects of the phase change on long-period waveforms are compared to observed waveforms in well-sampled regions of the lowermost mantle. Then, thermo-chemical models of the entire lower mantle are explored using a series of possible geotherms and transition depths to identify the conditions for which anomalous regions can be best explained by the presence of post-perovskite. Finally, both the effects of temperature and post-perovskite on shear and compressional velocity anomalies are taken into account to determine if post-perovskite can explain the anti-correlation of shear velocity and bulk sound speed near the base of the mantle.

2. NORMAL MODES

Very large earthquakes excite standing wave vibrations, or normal modes, throughout the Earth causing the Earth to "ring like a bell" for periods of hours to days. These normal modes are observed as peaks in the frequency domain representation of a seismogram. The spheroidal and torodial patterns of normal mode energy can be expressed in terms of spherical harmonics, S^m_l and T^m_l, where l is the degree of the harmonic and m is the order, $m = 2l + 1$. In theory, the spheriodal energy (*S*) should only appear on the vertical and radial components of a seismogram and likewise the torodial energy (*T*) should only be present on the transverse component of the seismogram. However, there can be coupling between the two due to rotation and 3-D structure [*Woodhouse,* 1980; *Masters et al.,* 1983] [for a more complete summary see *Masters and Widmer,* 1995]. Normal mode eigenfrequencies are optimal for constraining the 1D properties of the earth since they are intrinsic properties of a solid body and as such are unaffected by earthquake location and timing errors. In addition, normal modes provide the most reliable density estimates of any available seismic observations and are highly sensitive to even very small perturbations in the radial velocity and density profile of the earth. Here, the constraints that normal modes provide on the existence of post-perovskite in the lowermost mantle are examined.

To familiarize the reader with the lateral and depth sensitivities of certain normal modes, Figure 1 shows the lower-mantle sensitive modes S^m_2 and S^m_4 as functions on a sphere (top) and their shear (solid line) and compressional (dashed line) sensitivities as a function of depth (bottom). To conserve space, only the patterns for $-1 \leq m \leq 1$ are shown. As the value of l increases, the pattern on the sphere becomes more complex. The Earth resonates with the same spherical harmonic pattern at specific frequencies. The notation ${}_nS_l$ indicates the overtone index, n, for a given harmonic degree, l. The fundamental mode ${}_0S_l$ is the lowest frequency mode occurrence and modes that occur at higher-order frequencies are termed overtones. Mode energy may not be observed at all if it is trapped at an interface such as the CMB (i.e. a Stoneley wave). The fundamental modes typically

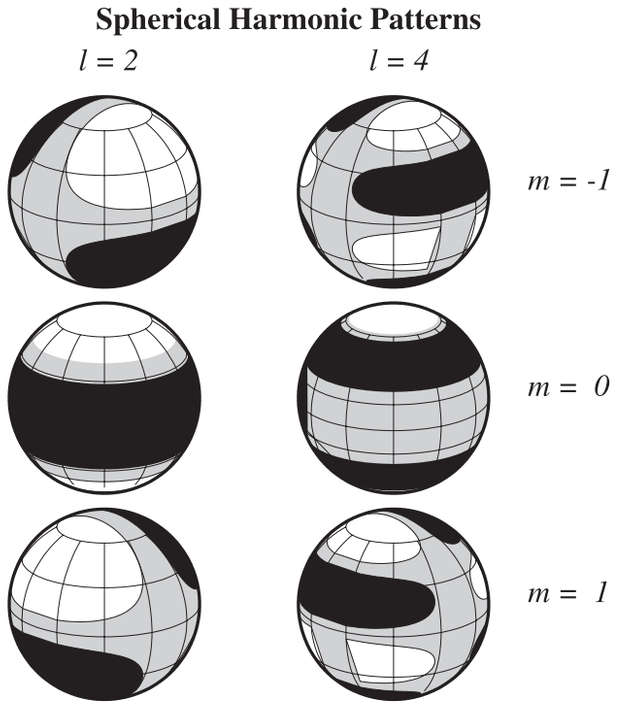

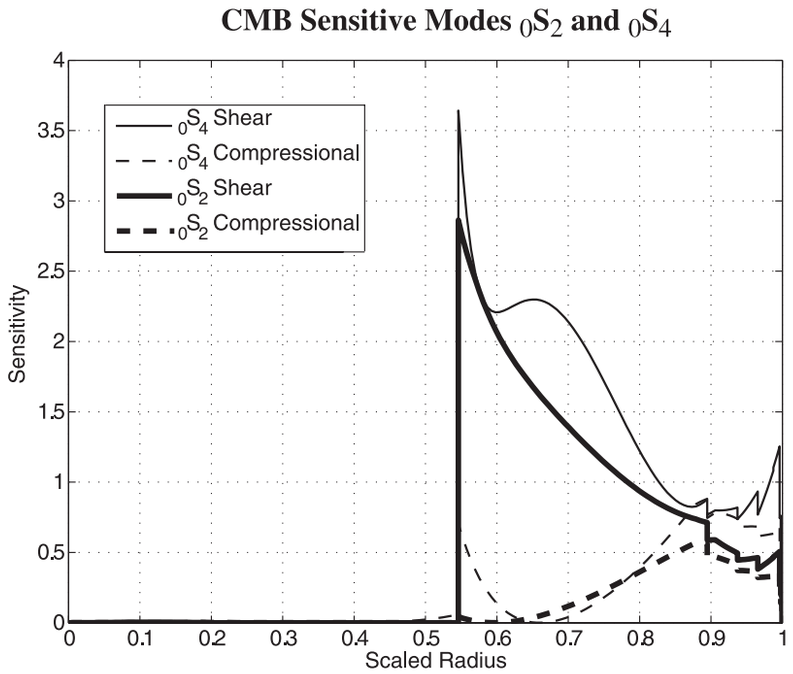

Figure 1. Top: Radiation pattern of fundamental modes ${}_0S^m{}_2$ and ${}_0S^m{}_4$ expressed as spherical harmonics for $-1 \le m \le 1$. Bottom: Depth sensitivity of ${}_0S^m{}_2$ (bold lines) and ${}_0S^m{}_4$ (grey lines) as a function of radius where $r = 1.0$ at the Earth's surface and $r = 0.55$ at the CMB. The modes are dominantly sensitive to shear velocity structure near the CMB.

represent surface wave behavior while the overtones are generally equivalent to body waves. However at low *l*, the fundamental modes have much of their energy concentrated near the CMB (Figure 1). Thus, it is mainly these low harmonic degree, low overtone-index modes that provide constraints on the radial velocity and density structure near the CMB.

Since normal modes are uniquely suited for constraining the 1D structure of the Earth, they can be used to explore possibilities (1) and (2) that post-perovskite either exists everywhere or not at all in the lowermost mantle. The modes shown in Figure 1 are mainly sensitive to structure on the mantle side of the core-mantle boundary, however a tiny fraction of the ${}_0S_2$ shear energy is in the inner core and a small amount of ${}_0S_4$ compressional energy is present in the top of outer core. This non-localization of energy makes it difficult for normal modes to constrain the one-dimensional velocity and density structure at the core-mantle boundary. Figure 2 shows the ability of the normal mode degenerate frequency estimates compiled by *Masters and Gubbins* [2003] to resolve the average radial compressional velocity (top), density (middle), and shear velocity (bottom), throughout the mantle. To construct Figure 2, the averaging kernels [*Backus and Gilbert*, 1968] are computed by specifying a desired error level and solving for the kernel width (the averaging length). The kernel widths are computed at every 200 km in the mantle and reveal the ability of the normal modes to resolve structure at the desired error level. An example of the averaging kernels is shown in the inset at the bottom of Figure 2 for a radius of 3700 km. Rather than display a myriad of averaging kernels; the widths of the kernels as function of radius in the mantle are plotted for errors of 0.1% (dashed line), 2% (solid line), and 5% (dash dot line). That is, the modes are able to resolve the average 1D shear velocity within an error of 2% at a radius of 3700 km (220 km above the CMB) when the average is taken over a radial zone 250 km wide (bottom inset). The width of the radial zone over which the average applies increases to 450 km (bottom inset) if the desired error level decreases to 0.1%. Thus, there is a tradeoff between the accuracy of the velocity and density measurements and the depth range (i.e. kernel width) over which the average must be computed to achieve a particular level of accuracy.

Near the CMB, the slope of most 1D shear and compressional velocity curves decreases. This feature of the deep mantle was first identified by *Bullen* [1949] and defined as the D″ region. Within D″, the velocities are slower than would be consistent with adiabatic increases in temperature and pressure for the depths of the lowermost mantle. Thus, this region has been interpreted as a thermal boundary layer indicating a large temperature jump across the CMB. With the discovery of the post-perovskite phase, it is necessary to question if a global velocity increase could occur within D″, however, without detection by the normal modes. Figure 2 demonstrates the work of *Masters and Gubbins* [2003] that the width of the radial zone required to achieve accuracy within a given error level increases dramatically near the CMB for shear velocity (top), decreases for compressional velocity (middle), and remains fairly level for density (bottom). While the 1D compressional velocity is better constrained near the CMB than the shear velocity, the predicted effects of the Pv to pPv transformation on the compressional velocity is smaller (~0.5%) than that predicted for shear (~2%). Thus, in order for a global layer of post-perovskite to be present in the lowermost mantle and lie below the detection threshold of the normal mode data, it would have to occur within approximately 200 km of the CMB.

The consideration of the 1D normal mode constraints is important to our understanding of post-perovskite because unlike reflected phases, their ability to detect the transition is not hindered by the sharpness (or lack thereof) of the transition. In addition, their ability to detect the transition increases as the transition moves to lower pressures. The errors on the pressure (hence depth) of the Pv to pPv transition are on the order of 5 - 10 GPa or 100 – 200 km. Theoretical and experimental studies [*Akber-Knudsen et al.,* 2005; *Tateno et al.,* 2005] have indicated that the inclusion of Al in pPv structure can broaden the phase loop of the perovskite to post-perovskite transition, decreasing the amplitude (hence detectability) of reflections from the transition. It was originally proposed that increasing Fe shallows the transition [*Mao et al.,* 2004], however *Hirose et al.* [2006] suggest that this difference may result from the use of different pressure scales. The experimentally determined transition of Pv to pPv for a pyrolite composition [*Murakami et al.,* 2005] and a MORB composition [*Hirose et al.,* 2005] using the Au pressure scale [*Tsuchiya,* 2003] occurs at about 110 GPa for an adiabatic geotherm [*Williams,* 1998] or a depth of about 350 km above the CMB. Phase transitions measured for pure $MgSiO_3$ using the Pt pressure scale [*Holmes et al.,* 1989] or the *Jamieson et al.* [1982] Au pressure scale occur at depths within 200 km of the CMB [*Murakami et al.,* 2004; *Oganov and Ono* 2004; *Ono and Oganov*, 2005]. The studies corresponding to a deeper transition are consistent with the majority of observations of reflectors in D″ [*Wysession et al.,* 1998]. The fact that the normal modes do not detect a velocity increase at depths shallower than 2680 km indicates that either Fe does not have a major effect the transition pressure or that there is not enough Fe in the lowermost mantle to produce sufficient shallowing of the transition such that the entire region is within the post-perovskite stability field. Also, the normal modes favor the experimental studies that find the Pv to pPv transition likely occurs in close proximity to the CMB.

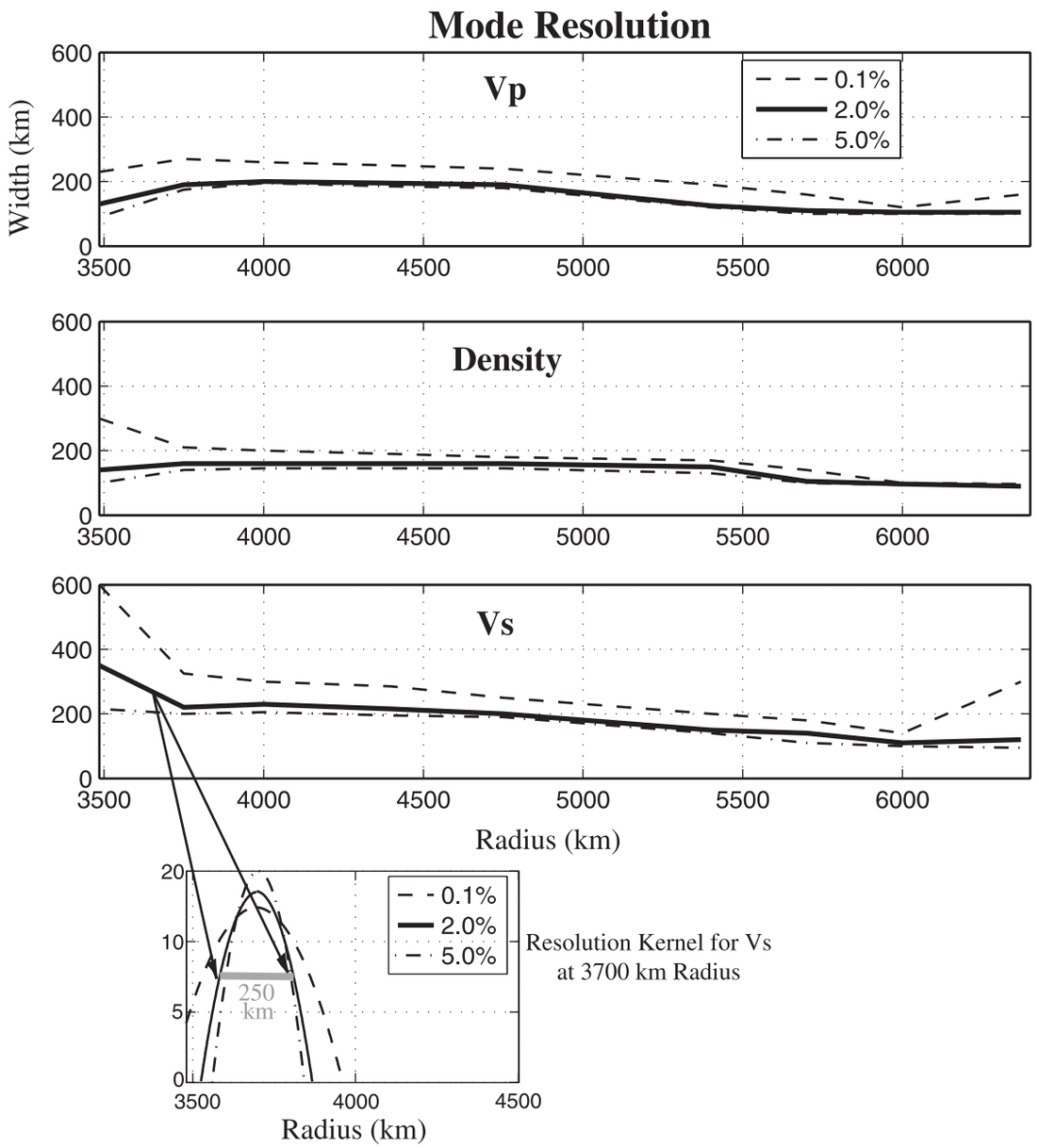

Figure 2. Width of the mode resolution kernel for compressional velocity (top), density (middle), and shear velocity (bottom) for error levels of 0.1% (dashed line), 2.0% (solid line), and 5.0% (dash-dot line) as a function of radius in the mantle. At a particular radius, as the error level decreases, the width of the zone required for the mode data to resolve the average velocity or density at that level of error increases. The bottom inset shows the actual Backus-Gilbert averaging kernels for the shear velocity at 3700 km radius. The width of the kernel (shown in grey) for a 2% error level is 250 km.

In summary, if the post-perovskite phase is a ubiquitous phase at some depth in the lowermost mantle, it must be confined below 150 – 200 km above the CMB, or else it would be detected by the free oscillations of the earth. Since it has been demonstrated that the normal modes have reduced sensitivity near the CMB, it is necessary to examine the long-period waveforms for signs of a global Pv to pPv transition at depths greater than 2680 km.

3. LONG-PERIOD WAVEFORMS

The majority of evidence thus far for a Pv to pPv transition in the lowermost mantle has come from short-period seismic studies that find discontinuous jumps in seismic velocity within a couple hundred kilometers of the CMB [*Thomas et al.,* 2004a,b; *Chambers and Woodhouse*, 2006; *Sun et al.,* 2006; *Hutko et al.,* 2006; *van der Hilst et al*., 2007]. These short-period studies use stacking procedures to determine if there is any coherent signal that can be related to reflections off of a seismic discontinuity. This type of methodology can be applied in locations where there is enough data redundancy to allow small amplitude reflections to emerge out of the background noise level. Reflectors were first observed in the D″ region by *Lay and Helmberger* [1983]. Since then, the majority of D″ reflectors have been identified in fast regions that are thought to be associated with ponding of subducted lithospheric slabs at the CMB. The velocity increase associated with these reflectors is often explained in terms of chemical heterogeneity [see *Wysession et al.,* 1998 and *Lay and Garnero*, this volume, for a summary and further details]. When the Pv to pPv transition was first discovered to have a steep, positive Clapeyron slope, it seemed probable that the reflections observed in these fast, likely cold, regions were due to the cold thermal anomaly of the slab placing the region in the pPv stability field. This interpretation suggests that fast regions at the CMB are fast not only because they are cold, but also because of the transition to post-perovskite. Likewise, slow regions may be slow because they are too warm for post-perovskite to exist, and are possibly chemically distinct as well. This simplistic view has recently been challenged as velocity jumps in the D″ region have also been identified in tomographically slow regions [*Avants et al.,* 2006; *Lay et al*., 2006; *Lay and Garnero*, this volume]. For post-perovskite to exist in these slow regions there must be strong chemical heterogeneity to overcome the effects of the increase in temperature. Thus, it would be advantageous if long-period seismology could provide a comprehensive understanding of the relation between post-perovskite and fast and slow areas at the CMB.

In this section, the predicted effect of post-perovskite on long-period waveforms is determined and compared to actual data. Long-period waveforms of phases such as *S*, *P*, and *ScS* are too broad for reflections from an interface with a small velocity contrast to be detected. However, the velocity increase associated with the phase transition will result in a distortion of the long-period travel-time curve. The arrival times for a series of synthetic seismograms are shown in Figure 3. The synthetics were calculated based on actual ray paths turning in a 4° diameter circular bin in the north-central Pacific (longitude = 190, latitude = 21). The traces range from distances of 85° - 100° at a roughly 0.2° interval. This region was chosen due to the high concentration of turning points in the lowermost mantle (see Plate 1). The synthetics of the observed seismic traces are computed using normal mode summation for a dominant period of 20 seconds consistent with the long-period dataset. The left hand plot of Figure 3 shows the arrival times of seismograms computed with the isotropic PREM [*Dziewonski and Anderson,* 1981] 1D reference Earth model. The arrival times on the right hand side are from seismograms computed using a modified version of PREM, which has a 2% jump in shear velocity and density and a 1% jump in compressional velocity 180 km above the CMB. This depth was chosen as it is deep enough to be within the uncertainty of the normal mode data and is consistent with the majority of experimental and theoretical studies regarding the depth of the Pv to pPv transition [*Hirose*, 2006]. Both sets of arrival times are aligned on the predicted PREM arrival. The shear velocity jump in the altered 1D model clearly causes the *S* wave pulses to arrive earlier than those predicted by PREM for distances beyond ~92°. This shift or bend in the travel-time curve is easily

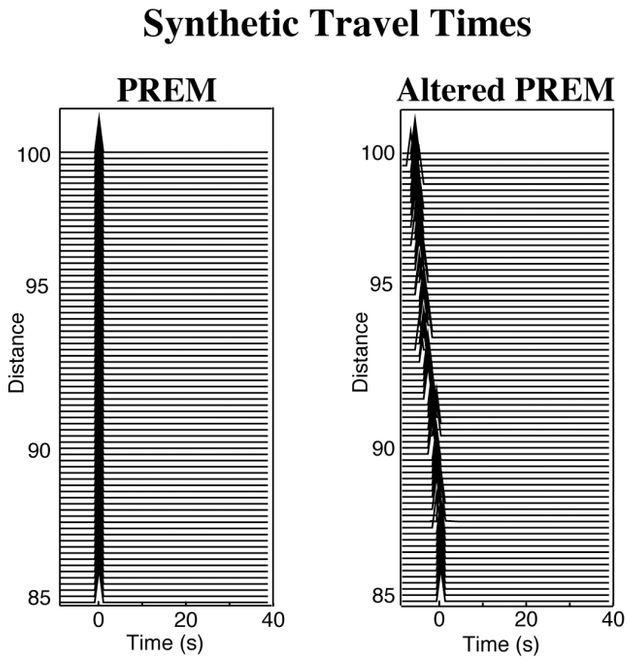

Figure 3. *S* wave arrival times of synthetic seismograms calculated using isotropic PREM (left) and an altered version of PREM with a 2% shear velocity increase at 180 km above the CMB. The traces span from 85° – 100° with a 0.2° spacing and are aligned on their PREM predicted times. The negative shift or bend in the travel-time curve of the altered PREM model begins at approximately 92°.

detectable and would be apparent in observed seismograms where there are numerous turning rays. It is important to note that the phase transition would have to occur at a depth high enough above the CMB that the bend in the travel-time curve could be detected. Therefore, even if a bend in the travel-time curve is not observed, post-perovskite could still exist at depths within about 50 km of the CMB. However, depending on the magnitude of the thermal boundary layer, it could be too hot for post-perovskite to be stable so close to the CMB.

The following is a description of the procedure for the global analysis of long-period travel-time curves. (1) The subset of arrival times corresponding to rays in the *Houser et al.* [2007] cluster analysis catalog of long-period *S* arrivals (spanning from 1976-2005) that turn in a distance range of 85° – 100° are collected. In addition, the arrival times for deep-turning, high signal-to-noise *S* phases not currently in the *Houser et al.* [2007] catalog are determined by manual cross-correlation with a synthetic *S* phase, similar to the technique described in *Bolton and Masters* [2001]. These manually determined arrival times are used to supplement the cluster analysis catalog in order to have the most complete dataset of long-period travel times for deep turning rays. All of the times have been corrected for ellipticity, crustal structure using CRUST 2.0 *(Laske et al.* http://mahi.ucsd.edu/Gabi/rem.dir/crust/crust2.html), and upper mantle velocity structure using HMSL - S06. (2) The arrival times of the *S* waves are binned according to their respective turning points within 4° diameter circular bins at intervals of 2°. (3) The arrival times are visually inspected bin by bin to identify if there is a negative (fast), positive (slow), or no observed bend in the travel-time curve. The distance at which the bend occurs and the magnitude of the bend are measured if a bend in the travel-time curve exists.

The resulting map of fast (blue) and slow (red) bins is shown in Plate 2. The bins in which the travel-time curve is straight are left white. The "null" observations indicate that the arrival times are too scattered to discern any bend in the travel-time curve and are shaded grey. An interesting feature of Plate 2 is the small number of bins for which any bend in the travel-time curve can be detected. There are around 270 bins in which the distribution of the turning rays spans the distance range of 90° – 100° necessary to distinguish a bend in the travel-time curve near the CMB. In approximately half of these bins, the travel times are too scattered to discern whether or not a bend occurs (grey regions, Plate 2). In the remaining 160 bins which have a well-defined travel-time curve, only about 45 have a measurable negative bend (i.e. fast), and only around 20 bins have a measurable positive bend (i.e. slow). Thus, an overwhelming majority of these bins (around 95) have no bend in the travel-time curve. While these straight travel-time curves may already be fast or slow with respect to PREM, they indicate there is no further velocity increase or decrease within 200 km of the CMB in these regions.

Actual observed travel-time curves within bins with a negative bend (fast), a positive bend (slow), and no bend are shown in Plate 3. The median time offset for the slow and fast regions is ±4 seconds, corresponding to velocity variations on the order of ±2%. The median distance at which the times begin to sense fast and slow material occurs at around 92° or 180 km above the CMB. The large number of bins in which there is no deviation in the travel-time curve indicates that if post-perovskite does exist in the lowermost mantle, it may be a localized phenomenon. The null bins are not completely devoid of information as there are patterns that may indicate abrupt velocity variations. For instance, there are regions in which two parallel travel-time curves exist separated by a few seconds. This splitting of the travel-time curve could indicate rapid lateral velocity variations within these bins. Furthermore, although the null measurements appear to be evenly distributed, there are areas (such as central Eurasia) where they are the dominant travel-time pattern.

The blue bins representing fast travel times within 100 km of the CMB in Plate 2 are concentrated under Alaska, Northern Eurasia, and the Cocos plate. These areas are characterized by broad fast velocity anomalies within the bottom 600 km of the mantle in tomographic models. The shear velocity model of *Houser et al*. [2007] is shown in Plate 4 for comparison. The observation of a further increase in velocity near the CMB within these tomographically fast regions supports the idea that the cold thermal anomaly of ancient subducted slabs causes the transition of Pv to pPv. However, a concentrated region of fast travel-times is located in the tomographically slow region of the central Pacific where most of the slow travel-times are located. *Avants et al.* [2006] also observe sharp increases in velocity within the tomographically slow region to the south of Hawaii. Therefore, the observation of relatively fast material in these predominantly slow regions may reflect local chemical anomalies that are favorable for the Pv to pPv transition.

Thus, the overall conclusion from the long-period travel-times is that post-perovskite is not a global feature within 200 km of the CMB. However, the presence of post-perovskite can explain observed increases in shear velocity within tomographically fast regions in the lowermost 100 km of the mantle. In addition, relative velocity increases are found within tomographically slow regions. This demonstration that post-perovskite is likely present in some of the best-sampled areas of the lowermost mantle implies that it may be present in the other anomalous regions of the CMB as well. Therefore, the ability of seismic tomography to constrain the presence of post-perovskite throughout the entire lower mantle is explored in the next section.

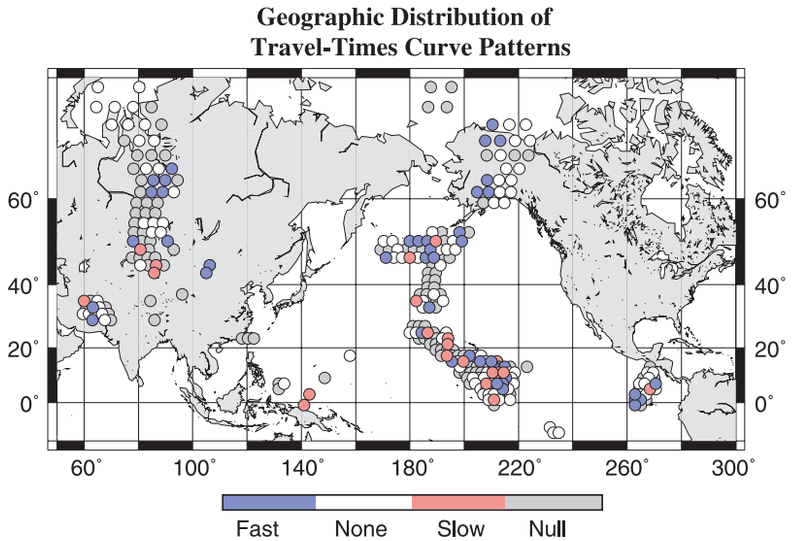

Plate 2. The geographic distribution of bins in which fast (blue), slow (red), or no (white) trends are observed in the travel-time curve of long-period *S* arrivals. Grey bins indicate the null observations where no trend was discernable from the data. Areas outside of the frame do not have the density of ray coverage to be used in this analysis. The clustering of fast arrivals under Alaska and the Cocos plate may signal the presence of post-perovskite. The juxtaposition of fast and slow bins in the central Pacific is required by the data and indicates rapid lateral variations that may by due to pockets of post-perovskite in this generally slow seismic region.

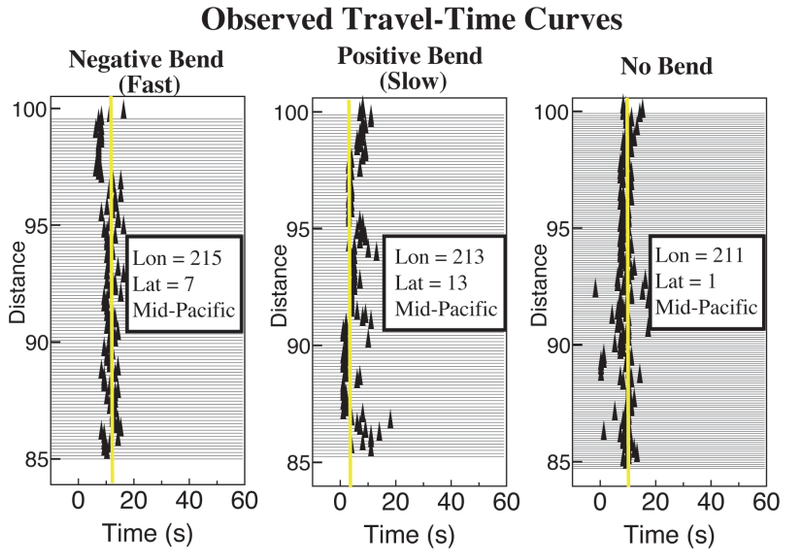

Plate 3. Examples of the travel-time curves from bins in which a fast trend (left), slow trend (middle), or no trend is observed in the long-period *S* wave arrivals. The vertical yellow lines are provided as guides for determining the overall vertical trend in the data.

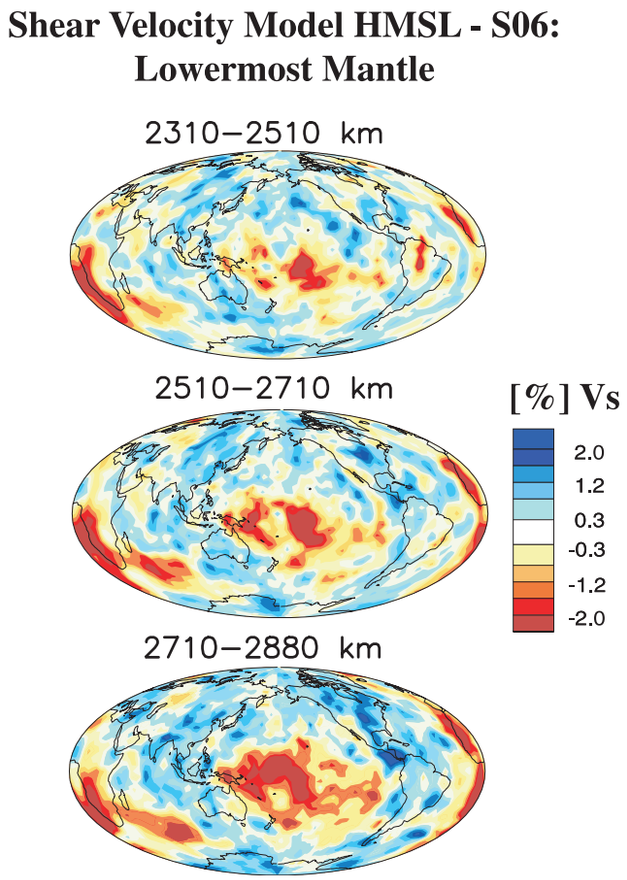

Plate 4. Depth slices of the bottom 500 km of the shear velocity model, HMSL – S06, from *Houser et al.* [2007]. Dark blues and reds are 2% fast and slow respectively. The model is constrained near the CMB by the combination of direct *S* and core-reflected *ScS* phases.

4. SEISMIC TOMOGRAPHY

The long-period waveforms reveal that regions of the lowermost mantle have fast shear wave velocities consistent with that expected for post-perovskite. However, there is limited coverage with direct *S* arrivals as shown in Plate 1. Thus, to investigate lateral variations of post-perovskite on a global scale, it is necessary to investigate tomographic models for their ability to reveal the occurrence of post-perovskite. Tomographic models simply map where seismic wavespeeds are slower or faster than the average speed at that depth. Since the late 1970s, tomographic models have imaged slow shear and compressional anomalies beneath the Pacific and Africa and fast anomalies in the circum Pacific near the CMB [*Sengupta and Toksov,* 1976; *Dziewonski et al.,* 1977; *Clayton and Comer,* 1983; *Dziewonski,* 1984; *Hager et al.,* 1985]. With the finding that post-perovskite is a seismically fast phase, it is necessary to evaluate whether or not the fast anomalies near the CMB are associated with the phase transition. Here, a different approach is used in which possible depths of the phase transition and previously published geotherms are explored using thermo-chemical models based on seismic data to determine if fast anomalies in the lowermost mantle are consistent with the presence of post-perovskite.

Recent mineralogical studies have developed P-V-T equations of state for perovskite [*Trampert et al.,* 2001, *Mattern et al.,* 2005, *Li and Zhang,* 2005]. These equations of state are used to extrapolate seismic velocities and density to lower mantle temperatures and pressures. By altering the initial conditions, such as the temperature or concentration of iron, and performing a series of extrapolations, the changes in seismic velocity with temperature and composition can be determined [*Trampert et al.,* 2004; *Li*, *in preparation*]. The dominant signals in the lowermost mantle are the variations in shear velocity [*Houser et al.,* 2007] as shown in Plate 4. Therefore, interpretations of lowermost mantle thermo-chemical structure will be most dependent on the values of the change in shear velocity with temperature ($d \ln V_S / dT$) and the change in shear velocity with composition ($d \ln V_S / dX$). Using these derivatives, a tomographic inversion can be reframed to directly solve for the nature of thermo-chemical anomalies [*Trampert et al.,* 2004; *Reif et al.,* 2005]. The values of $d \ln V_S / dT$ from the *Trampert et al.* [2004] study are much less than those of Li [*in preparation*] resulting in very different thermo-chemical models. Essentially, density anomalies are mapped into variations in iron in the *Trampert et al.* [2004] model due to larger values of $d \ln \rho / dX_{Fe}$ than $d \ln V_S / dT$, while shear velocity is mapped into variations in temperature in the *Reif et al.* [2005] model since $d \ln V_S / dT$ is greater than $d \ln \rho / dX_{Fe}$. In these studies, the 3D density structure is only constrained by the normal mode structure coefficients developed from measurements of mode splitting. *Trampert et al.* [2004], *Beghein et al*. [2002], and *Ishii and Tromp* [2001, 2004] all find that the modes reveal a degree two pattern in the lowermost mantle of density excess in the vicinity of the slow shear velocity anomalies under the Pacific and Africa. However, *Masters et al*. [2000] finds that when the body waves are combined with the 3D mode structure coefficients to constrain the shear and compressional velocity structure of the lower mantle, then the density signal is very weak. Thus, differences in the thermo-chemical models also arise from the different datasets used in the inversions.

This study is not meant to evaluate which set of values is most likely to represent the lower mantle, but to use these values to construct end-member models of temperature and composition. The *Reif et al.* [2005] model is based on an extensive body wave dataset as opposed to the model of *Trampert et al.* [2004] which has only 3 layers in the lower mantle, and coarser lateral parameterization since it is based purely on normal mode data. To aid in comparison, the sensitivities used by *Trampert et al.* [2004] are applied to the *Houser et al.* [2007] dataset of *S* and *P* body waves as well as measurements of normal mode splitting coefficients [*Masters and Gubbins*, 2003] to invert for lowermost mantle thermo-chemical structure. The resulting two models of lowermost mantle temperature and composition are shown in Plate 5. The top two rows contain the deepest layers of the model which is dominated by temperature variations [*Reif et al.,* 2005] (hereafter referred to as Model A), and the bottom two rows contain the deepest layers of the model which is dominated by variations in the mole fraction of iron (based on *Trampert et al.* [2004]), (referred to as Model B).

Models A and B share the characteristic that the pattern of heterogeneity in the parameter that is dominantly sensitive to shear velocity reflects the overall pattern of the shear velocity model. In places such as the central Pacific where *S* and *P* velocities are not consistent with purely thermal or chemical effects [*Masters et al.,* 2000; *Forte et al*., 2001; *Ishii and Tromp,* 2004], additional heterogeneity is required in the other parameters to explain the data. For instance, in Model B the iron variations look very much like the shear velocity anomalies, but under the central Pacific and Africa, high temperatures accompany the increases in iron in order to be able to explain the data. One main difference in the models is that little structure is present in the iron map of Model A and the perovskite map of Model B, due to the different sensitivities of the two models. Another important difference is the change in magnitude of the iron and temperature variations from Model A to Model B. Since Model A is dominantly sensitive to temperature, a smaller change in temperature is necessary to create the same change in shear velocity compared to Model B. Likewise, the magnitude of the iron variations in Model B is smaller than that in Model A. The counter-intuitive result is

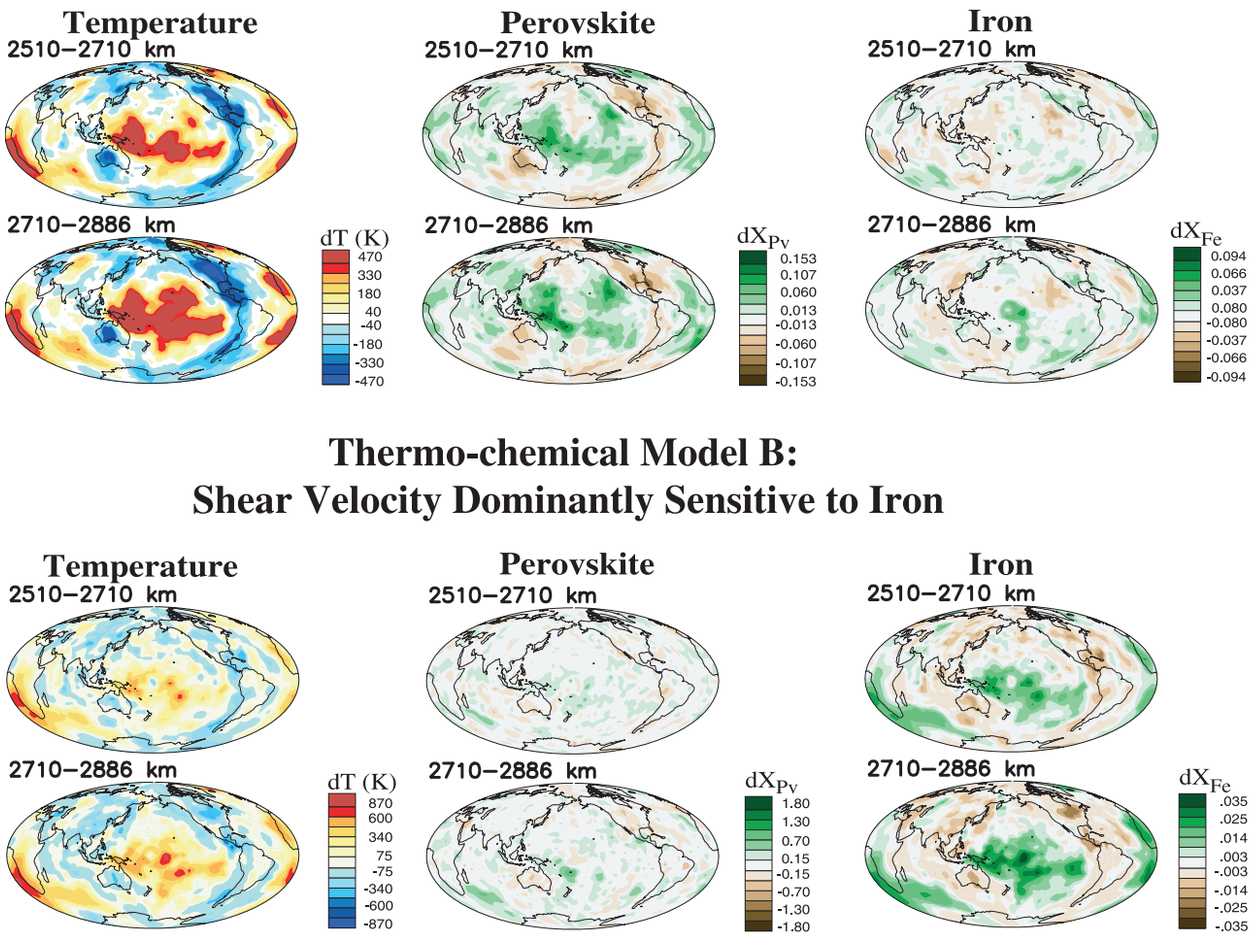

Plate 5. Depth slices of thermo-chemical models computed by applying different sets of shear and compressional wave and density sensitivities to temperature and the mole fractions of perovskite and iron in the lower mantle. The seismic and density data for both models consist of a combination of shear and compressional body waves and normal mode splitting coefficients. Model A (top rows) uses the sensitivities of *Li* [*in preparation*] in which shear velocity is dominantly sensitive to temperature fluctuations. Model B (bottom rows) is the result of using the sensitivities used in *Trampert et al.* [2004]. The scales on the perovskite and iron content are the mole fraction variations. The scales of both the temperature and chemical variations differ for the two models such that the maximum and minimum on each scale represents the amount of variation in that parameter necessary to produce a shear velocity anomaly of ±2%. Thus, each thermo-chemical parameter is plotted at essentially the same scale as the shear velocity model shown in Plate 4.

that the model, which is less sensitive to a given parameter, will have larger fluctuations in that parameter. Thus, although Model A is dominantly sensitive to temperature, the temperature variations are larger in Model B. The scales for Models A and B are different because they are all normalized such that the minimum and maximum of the temperature and composition scales will produce a ±2% shear velocity anomaly. Since Model A is dominantly sensitive to temperature, a smaller increase in *dT* will produce a 2% shear velocity anomaly than that required for Model B. This normalization reveals the relative contribution of each thermo-chemical parameter to the change in shear velocity for a given set of input parameters. Thus, while the scales for Models A and B are very different, the magnitude of the variations in temperature and iron content are quite similar. Consequently, the patterns in the predicted lateral variations of post-perovskite obtained from applying the temperature variations from both models to assumed lower mantle geotherms are also similar.

The question addressed here is: where is post-perovskite predicted to occur in the lowermost mantle for a model of temperature and compositional variations given a suite of possible geotherms and Pv to pPv transition depths? This is accomplished by simply adding the temperature variations from the thermo-chemical models to an adiabatic mantle geotherm to calculate the absolute temperatures. Since the seismic data are demeaned prior to the inversion (see *Houser et al.* [2007] for details), they become independent of their 1D reference velocity model. Therefore, the 3D temperature and chemical variations can be added to any 1D temperature or chemical profile to obtain absolute values of temperature or chemical concentration. To obtain absolute values for iron abundance, the variations in the mole fraction of iron are added to the canonical value found to be suitable for most of the mantle, ~0.1 [*Ringwood*, 1982; *Jackson*, 1998; *Mattern et al.,* 2005]. Since the effects of silica content on the transition of perovskite to post-perovskite are not well documented and the thermo-chemical models suggest that silica is not likely to dominate variations in seismic velocities in the lowermost mantle, the effects of the silica variations in the models are ignored. The resulting model of absolute temperatures and values of the mole fraction of iron for the lowermost mantle is then used to produce a map indicating which regions would be in the Pv or pPv stability field for a sampling of possible phase transition depths.

While there is still disagreement regarding the depth of the Pv to pPv transition, to date, the experimental and theoretical mineral physics studies agree that the Clapeyron slope of the transition is rather steep. *Hernlund and Labrosse* [2007] provide a lower bound on the Clapeyron slope of the Pv to pPv transition by considering a range of acceptable inner core boundary temperatures, Pv to pPv transition depths, and temperatures in the lowermost mantle. Their findings indicate that the lower bound on the Clapeyron slope is around 8 MPa/K. The values reported by theoretical studies are in agreement that the slope is positive and in the range of 7 – 10 MPa/K [*Tsuchiya et al., 2004a*; *Oganov and Ono, 2004*]. *Hirose* [2006] finds the range in Clapeyron slopes from experimental studies to lie in the range of 5 – 11.5 MPa/K assuming different pressure scales. As the Clapeyron slope increases, the temperature anomaly required to shift a region in or out of the post-perovskite stability field decreases. Therefore, a high-end value, 11 MPa/K, is used here since it allows for the greatest lateral variation of post-perovskite for a given temperature field that is consistent with the current results of theoretical and experimental studies.

Thus far the following has been established: 1) The thermo-chemical Models A and B provide lower and upper estimates, respectively, on the magnitude of temperature variations near the CMB. 2) Applying these temperature variations to a mantle geotherm provides variations in the absolute temperatures near the CMB. 3) The highest acceptable value of the Clapeyron slope of the Pv to pPv transition maximizes the potential of a given temperature anomaly to shift Pv into the pPv stability field and vice versa. Therefore, given the Clapeyron slope of 11 MPa/K, the absolute temperature based on Models A and B, and the depth (i.e. pressure) of the Pv to pPv transition, it is possible to determine whether a region is predicted to be in the Pv or the pPv stability field. However, as previously discussed, there is much debate over the transition depth. To account for this uncertainty, the calculation is performed for a range of depths. Figure 4A shows the phase relationship between Pv and pPv for the upper and lower bounds on the range of depths of the Pv to pPv transition considered here (dashed lines) along with the *Brown and Shankland* [1981] adiabatic geotherm (solid black line). Figure 4B includes maps of the predicted occurrence of perovskite (white) and post-perovskite (grey) in the bottom layer of the mantle from the shallow (left) and deep (right) phase transitions in Figure 4A for Model A (top row), and likewise the bottom row is the result for Model B. When the shallow phase transition is applied to both models, the lateral temperature variations are not large enough to allow perovskite to be present, such that the entire layer at the CMB is in the post-perovskite stability field. Similarly, the lateral temperature variations are not large enough to allow post-perovskite to be present in the case of the deep phase transition such that the layer at the CMB is composed entirely of perovskite. The previous discussion on normal mode constraints concluded that post-perovskite is not a ubiquitous layer in the lowermost mantle, so the shallow bound on the transition depth is most likely too shallow. Figure 4 demonstrates that a transition depth that lies within the region bounded by the extreme shallow and deep Pv to pPv transition depths would be necessary to produce lateral variations for both Models A and B.

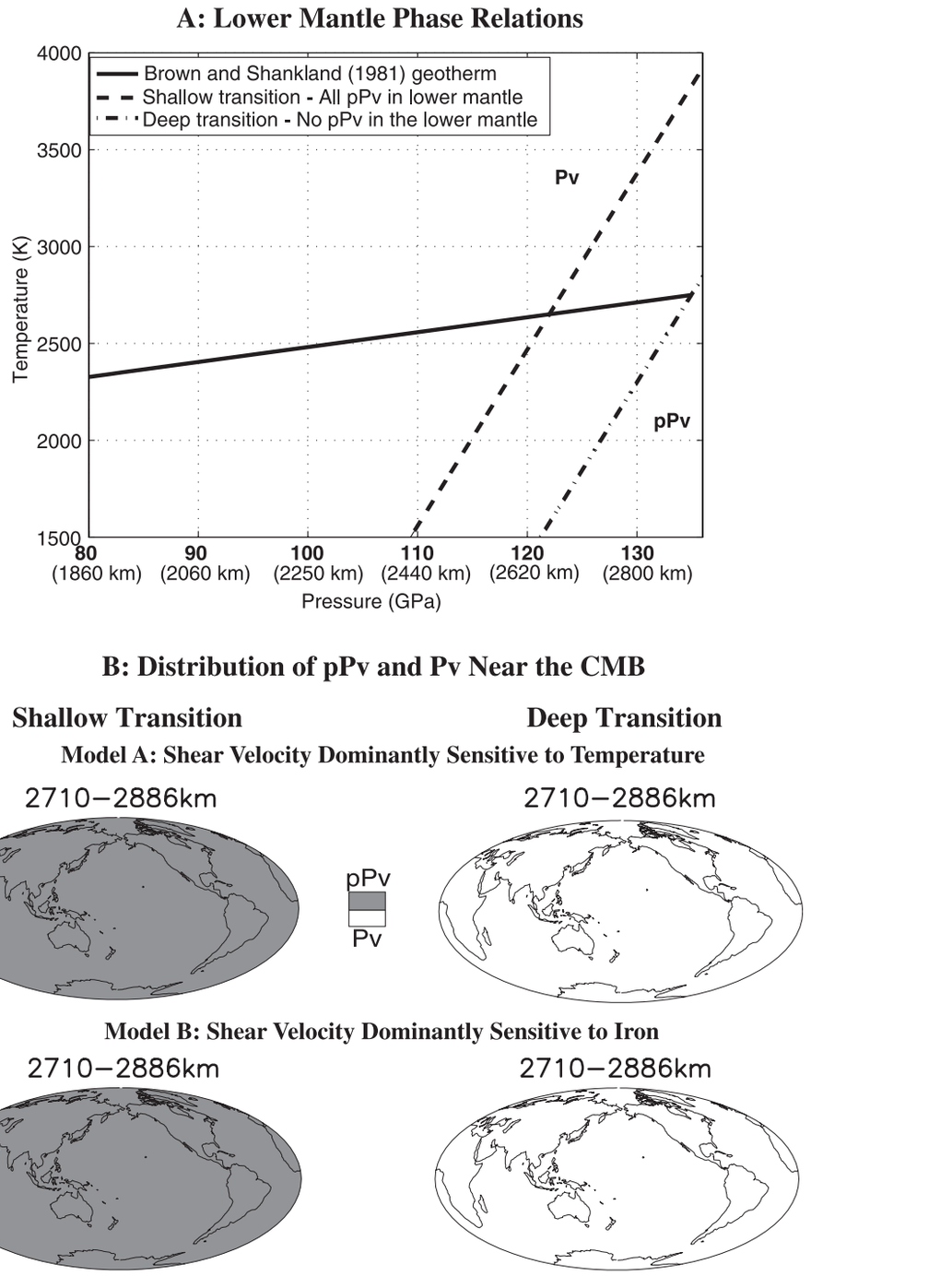

Figure 4. A: Phase diagram of the Pv to pPv transition assuming a Clapeyron slope of 11 MPa/K for the shallow (dashed line) and the deep (dash-dot line) bounds which predict pPv to exist either as a continuous layer or not exist at all near the CMB. Also plotted is the *Brown and Shankland* [1981] geotherm (solid line). B: Predicted locations of post-perovskite (grey) for the shallow transition (left) and the deep transition (right) given the temperature dominated Model A (top) and iron dominated Model B (bottom) shown in Plate 5. Any transition depth that lies between these bounds will result in lateral variations in post-perovskite.

The predicted lateral variations in the occurrence of post-perovskite in the bottom 200 km of the mantle using the *Brown and Shankland* [1981] geotherm, a Clapeyron slope of 11 MPa/K, and the temperature anomalies from Model A and Model B are shown in Figure 5. Figure 5B shows that post-perovskite is predicted to occur in the cold regions of both Models A (left) and B (right). This indicates that the presence of post-perovskite is not highly dependent on the difference in assumptions regarding the effects of temperature and composition on seismic velocities that were used to construct

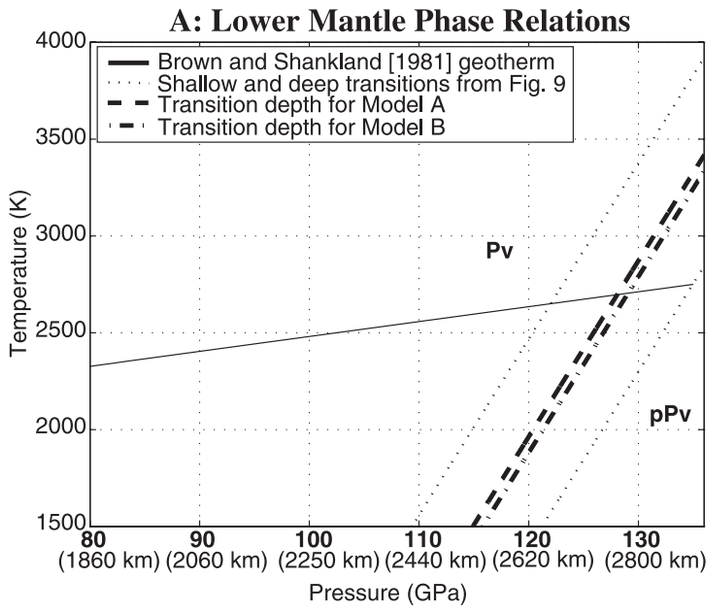

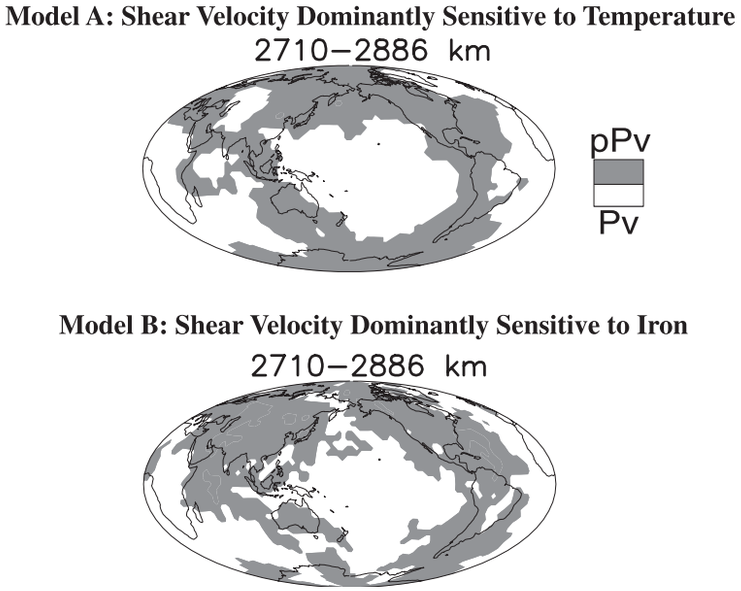

Figure 5. A: Phase diagram of the Pv to pPv transition assuming a Clapeyron slope of 11 MPa/K for depths that produce lateral variation in the occurrence of post-perovskite using the *Brown and Shankland* [1981] geotherm (solid line) for Model A (dashed line) and Model B (dash-dot line). B: Predicted geographic distribution of post-perovskite (grey) given the temperature dominated Model A (top) and iron dominated Model B (bottom) shown in Plate 5.

Models A and B. So far, the plots of the predicted variations in post-perovskite have been based on the *Brown and Shankland* [1981] geotherm. Figures 6-7 demonstrate that it is also possible to have lateral variations in post-perovskite for other geotherms. Figure 6A shows the high and low geotherms from *Williams* [1998]. The higher geotherm is calculated assuming a 1000K superadiabatic gradient across the transition zone, while the lower geotherm assumes no superadiabatic gradient across the transition zone. Note that the adiabatic *Williams* [1998] geotherm is similar to that of *Brown and Shankland* (1981). The predicted post-perovskite variations for Model A are shown in Figure 6B assuming the lower (adiabatic) geotherm (left) and the higher (superadiabatic) geotherm (right) for the respective transition depths that maximize the lateral variations in post-perovskite. The phase transition line used in the map of predicted post-perovskite for the low geotherm (6B left) is plotted as the dark dashed line in 6A while the phase transition line used in the map for the high geotherm (6B right) is plotted as the light dashed line in 6A. These two Clapeyron curves reflect possible uncertainties in the absolute depth of the transition, uncertainties induced by both pressure scales and the role of impurities. Figure 7 shows the results of applying the same methodology to the iron-dominated Model B. The phase transition depths for the low geotherm are the same for Models A and B, but a slightly deeper transition is necessary to produce

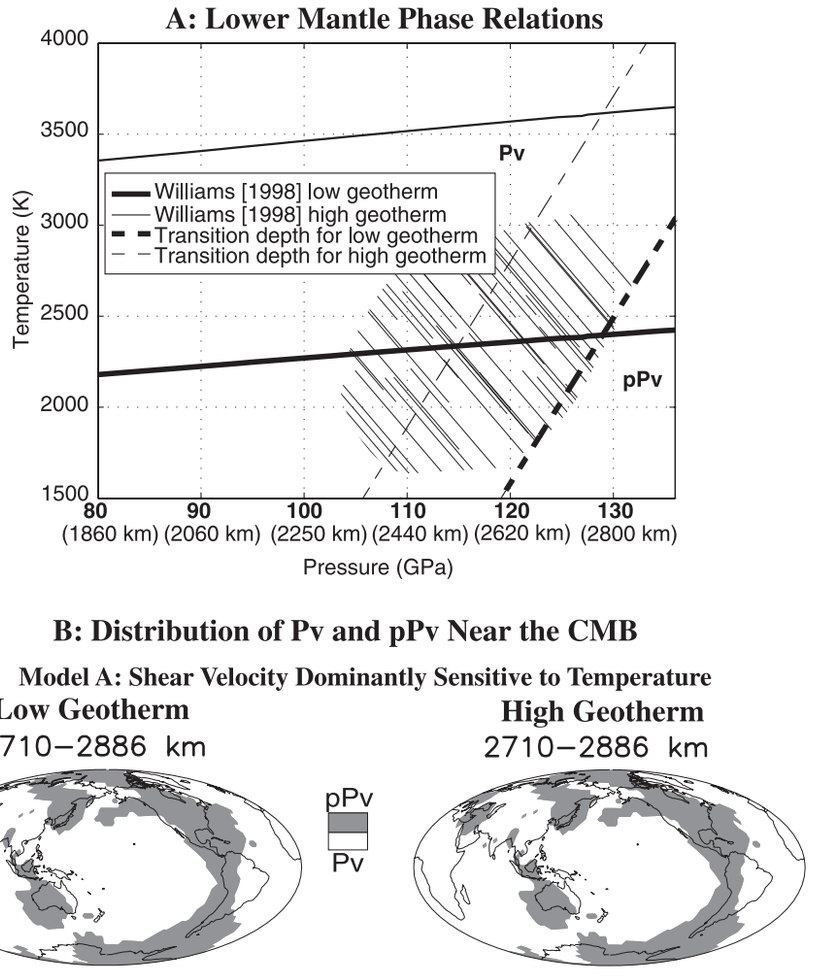

Figure 6. A: Phase diagram of the Pv to pPv transition assuming the Clapeyron slope of 11 MPa/K for a shallow transition (light dashed line) and a deeper transition (bold dashed line). The adiabatic (bold solid line) and superadiatic (light solid line) geotherms from *Williams* [1998] are also plotted. The hatched region indicates the P/T conditions for which the Pv to pPv transition has been observed experimentally, indicating that the lower geotherm is more consistent with experimental results than the high geotherm. B: The geographic distribution of pPv (grey) for Model A predicted by the adiabatic geotherm and deep phase transition (left) shown in 6A and by the superadiabatic geotherm and shallow phase transition (right) shown in 6A.

lateral variations for Model B using the high geotherm. Since there is little difference between Models A and B in the phase transition depths required to produce lateral variations in post-perovskite for a given geotherm, the differences in the magnitude of their respective temperature variations is not a primary factor in these calculations.

Since the tomographic models show that the fast anomalies in the lowermost mantle appear over 500 km above the CMB (Plate 4), they are likely a thermal feature. However, these fast velocities increase in magnitude at the CMB, suggesting an additional component affecting seismic velocities at this depth. It is widely assumed that the fast velocities at the CMB are due to the collective thermal and possibly chemical variations associated with subducted slab material. This analysis of the thermo-chemical models (based on body wave travel times and normal mode structure coefficients) finds that the additional velocity increase in the circum Pacific near the CMB could be due to the cold thermal anomalies shifting localized regions into the post-perovskite stability field. Thus, the fast anomalies result from a combination of thermal and mineralogical effects. From Figures 5-7, it becomes apparent that if one assumes that the fast regions of the mantle are fast due to the effects of post-perovskite, then this places rather tight constraints on the geotherm in the lowermost mantle as well as on the depth of the phase transition. The hatched region shown in Figures 6A and 7A encompasses the pressure

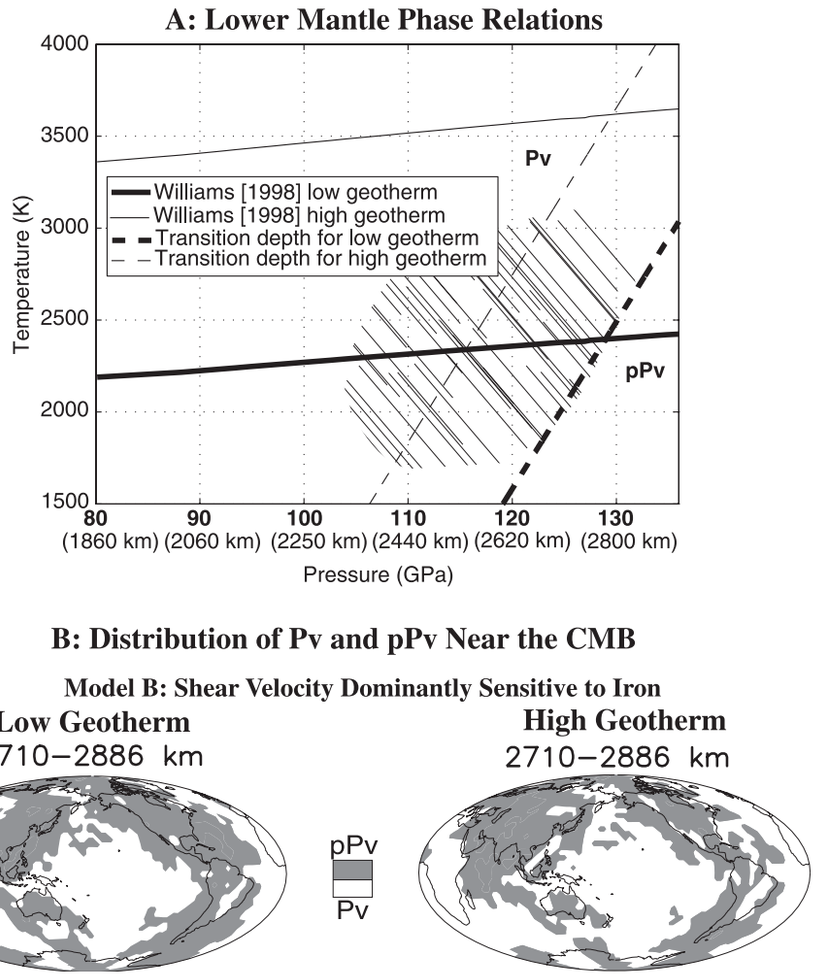

Figure 7. A: Phase diagram of the Pv to pPv transition assuming the Clapeyron slope of 11 MPa/K for a shallow transition (light dashed line) and a deeper transition (bold dashed line). The adiabatic (bold solid line) and superadiabatic (light solid line) geotherms from *Williams* [1998] are also plotted. The hatched region indicates the P/T conditions for which the Pv to pPv transition has been observed experimentally, indicating that the lower geotherm is more consistent with experimental results than the high geotherm. B: The geographic distribution of pPv (grey) for Model B predicted by the adiabatic geotherm and deep phase transition (left) shown in 7A and by the superadiabatic geotherm and shallow phase transition (right) shown in 7A.

and temperature range of the Pv to pPv transition from the variety of experimental studies summarized by *Hirose* [2006]. The experimental results obviously favor the lower, adiabatic geotherm from *Williams* [1998], if post-perovskite is present in the deep mantle. The Clapeyron slope (dark dashed line) representing the transition depth necessary to produce lateral variations in pPv given the lower geotherm boarders the deep edge of the hatched region defined by experimental studies. Thus, if the fast shear velocity anomalies are interpreted to be the combined effect of colder than average temperatures shifting the region into the pPv stability field, then the Pv to pPv transition occurs approximately at 2780 km depth (100 km above the CMB) and the temperature at this depth is approximately 2400 K. The depth remains the same, however, the temperature increases to 2700 K if the *Brown and Shankland* [1981] adiabatic geotherm is assumed (Figure 5).

It should be noted that the geotherms displayed here are adiabatic extending down to the CMB. Since the exact height and magnitude of the thermal boundary layer is unknown (but is currently being updated with investigations of the Pv to pPv transition [*Hernlund et al*., 2005; *Lay et al*., 2006]), the tomographic analysis here does not include speculations on the influence of the thermal boundary layer on the geotherm near the CMB. Consequently, the absolute temperatures calculated here based on the adiabatic geotherms can be considered a lower bound on the actual temperatures in the lowermost mantle (i.e. the most advantageous for the Pv to pPv transition). The velocity increases observed in the long-period travel time curves described in the previous section occur at depths of about 2780 km, which, if post-perovskite, indicates that large increases in temperature associated with the thermal boundary layer initiate at greater depths. Therefore, the lateral variations predicted for post-perovskite using the thermo-chemical tomography are likely valid for most of the depth range represented by the model layer above the CMB.

So far, this analysis has glossed over the effects of iron on the lateral velocity variations. To take into account the effects of elevated iron contents based on the *Mao et al.* [2004] study, if the absolute value of the mole fraction of iron in perovskite exceeds 0.15, the transition pressure is lowered by 2.5 GPa. The largest absolute values of the mole fractions of iron from Models A and B only approach 0.11 and 0.104 respectively for a 1D mole fraction value of 0.10. For the purpose of completeness, the analysis was redone with a range of average 1D values of the mole fraction of iron from 0.10 to 0.15. The lateral variations in iron do not have a significant effect on the lateral variations in post-perovskite until the 1D mole fraction value exceeds 0.14. However, once the 1D value of the mole fraction of iron is assumed to be this high, then the entire lowermost mantle should be in the post-perovskite stability field, according to the *Mao et al.* [2004] study. It has already been shown in the travel times that post-perovskite appears to be very localized. Thus, if it is assumed that the depth of the transition decreases as the iron content increases then such high values of the 1D-averaged iron content are inconsistent with the seismic observations.

The observation of fast travel-time curves in slow regions of tomographic models indicates that the iron content may vary locally on scales smaller than can be resolved by seismic tomography. Even the low estimates of $d \ln V_S / dX_{Fe}$ indicate that a 2% change in shear velocity would correspond to a mole fraction of iron in the neighborhood of only 0.16. Since the estimates of $d \ln V_S / dX_{Fe}$ are poorly constrained, it is possible that they are too high and that the magnitude of iron variations may be greater than that modeled here. Another possibility is that there are very large fluctuations in iron content over distances of only a few hundred kilometers that could lead to isolated pockets of post-perovskite. It is possible that post-perovskite would increase the shear velocity and thereby reduce the magnitude of the slow seismic anomaly attributed to iron, resulting in an underestimate of the relative increase in iron. However, the slow regions of the lowermost mantle are very slow and very broad features, such that pockets of post-perovskite will not affect the regional velocity structure enough to change the modeled variations in iron content by more than a few percent.

5. POST-PEROVSKITE AND THE ANTI-CORRELATION OF SHEAR VELOCITY AND BULK SOUND SPEED

Tomographic inversions that utilize both *S* and *P* data can jointly solve for shear and compressional velocity models, or can be reconfigured to jointly solve for models of shear velocity and bulk sound speed ($V_\Phi^2 = \kappa / \rho$) using the fact that $V_\phi^2 = V_p^2 - \frac{4}{3} V_s^2$ and consequently $d \ln V_\Phi = d \ln V_P - \gamma d \ln V_S / 1 - \gamma$ where $\gamma = 4V_S^2 / 3V_P^2 \approx 0.4$ for most of the mantle. Studies that have performed this exercise have found that in regions of the lowermost mantle where the shear velocity anomalies are very slow the bulk sound speed anomalies are fast, which is referred to as the anti-correlation between the two [*Masters et al*., 2000; *Antolik et al*., 2003; *Houser et al*., 2007]. It is important to note that this phenomenon is primarily the result of the shear velocity anomalies being much slower (-3 to -6%) than the compressional velocity anomalies (0 to -1%) in the Large Low Shear Velocity Provinces (LLSVPs). In these regions, an increase in incompressibility is needed to compensate the decrease in rigidity to account for the differences between shear and compressional velocities. *Karato and Karki* [2001] demonstrated that $R_{\Phi/S} = d \ln V_\Phi / d \ln V_S$ cannot be negative due to purely thermal anomaly since the Anderson-Gruneisen parameter, $\delta_S = d \ln \kappa / d \ln \rho$, does not likely fall below a value of 1.0 for lower mantle materials. Therefore, the anti-correlation of shear velocity and bulk sound speed anomalies in the lower

mantle is one of the main arguments for the seismic detection of chemical heterogeneity in the lowermost mantle.

This chemical interpretation of the anti-correlation has been brought into question with the discovery of post-perovskite, for which the low temperature estimates of elasticity intrinsically predict an anti-correlation, with regions of high shear velocity expected to have a decrease in bulk sound velocity. The basic argument is that the large shear velocity anomalies in the lowermost mantle are dominantly affected by lateral temperature variations and the Pv to pPv transition, such that the fast regions are cold enough to be in the post-perovskite stability field and the slow regions are warmer regions that remain perovskite. Thus, any intrinsic anti-correlation for the post-perovskite component affects the overall pattern detected by seismology and does not require variations in chemistry. Note that the anti-correlation will only be generated where post-perovskite is present; any anti-correlation in the warmer areas of perovskite must arise from some other effect, or from baseline uncertainties in the seismic models.

To test this proposition, here the relative behavior of shear and compressional velocity anomalies is explored taking into account 1) the tradeoff between temperature and post-perovskite on the shear and compressional velocity anomalies, and 2) the uncertainty in the sign of the V_P change as Pv transforms to pPv for high P-T conditions. In order to predict shear and compressional velocities, it is necessary to account for the effects of both temperature and post-perovskite on their variations. In the previous sections it has been established that if post-perovskite exists, it has to vary laterally in the lowermost mantle. It has also been established that the transition is more dominantly sensitive to temperature than composition, therefore, a function mapping temperature variations to shear velocity anomalies is developed. A recent study by *Helmberger et al.* [2005] converted the *Grand* [1994] model into depth variations of the Pv to pPv transition by converting shear velocity to temperature and using the 6 MPa/K Clapeyron slope inferred by *Sidorin et al.* [1999] from seismic data without taking into account the effect of the post-perovskite on the velocity anomalies. Here, both the effects of temperature and the phase change are accounted for using the following approach. Consider that the maximum shear velocity anomaly in the lowermost mantle is associated with a region that is composed entirely of post-perovskite and the associated temperature anomaly. Short-period seismic studies have found that the shallowest observation of the possible Pv to pPv reflector at ~350 km above the CMB [*Wysession et al.*, 1998]. Using this as the reference maximum thickness of post-perovskite and the Clapeyron slope of 11 MPa/K justified in the previous section, the decreasing thickness of post-perovskite as temperature increases outside this region can be predicted. The maximum velocity anomaly associated with the average of the bottom two layers (total height 380 km) of HMSL – S06 is 2.2%. However, tomography is not capable of recovering the entire amplitude of the actual velocity variations within the mantle, so a correction factor is applied which assumes that the recovered amplitude is 75% of the actual amplitude, bringing the maximum anomaly up to 2.9%. This value then is subdivided into a contribution from post-perovskite and temperature. The theoretical studies indicate that the Pv to pPv transition has at least a 2% anomaly in shear, so the rest of the anomaly is due to temperature. Since the absolute temperatures in the lowermost mantle are not known, the region of all post-perovskite is chosen as the baseline temperature, T_0. Then, using the mid-range value, $-4x10^{-5}$, of the $d \ln V_S / dT$ estimates that currently exist in the literature [*Trampert et al.*, 2004; *Stixrude and Lithgow-Bertelloni*, 2005; *Li* in preparation], the decrease in $d \ln V_S$ can be calculated for a given temperature increase dT. In addition, the post-perovskite contribution to the shear velocity anomaly decreases with dT as the thickness of the post-perovskite layer decreases according to the Clapeyron slope. We use the simple assumption that the tomography averages over the lowermost 380 km of the mantle, such that the contribution to the velocity anomaly is proportional to the thickness of the post-perovskite layer. The temperature and post-perovskite contributions are combined to develop the function of $d \ln V_S$ versus dT shown as the thick solid line in Figure 8A with the associated thickness of the post-perovskite layer displayed in Figure 8B. The coupled behavior of temperature and post-perovskite layer contributions to the shear velocity anomaly essentially produces a stronger effective $d \ln V_S / dT$ coefficient. In order to match the range of observed velocity anomalies, dT range of 1800 K is required, by which the post-perovskite layer has thinned to just a few tens of kilometers. Greater temperature variations would eliminate the post-perovskite layer and further changes in velocity would be proportional to the true temperature coefficient alone.

Since the mineral physics community has not reached a consensus as to whether V_p is higher, lower, or unchanged in pPv relative to Pv for high P-T conditions, each of these scenarios is explored here. Figure 8C shows the mapping of $d \ln V_P$ to temperature taking into account the post-perovskite thickness and the mid-range $d \ln V_P / dT$ of $-1.5x10^{-5}$ for each of these scenarios, the thick solid line represents a 0.5% increase in V_p and the thick dashed line represents a 0.5% decrease in V_p for the Pv to pPv transition; this represents the current range of uncertainty [*Stackhouse et al.*, 2005; *Wentzcovich et al.*, 2006]. The reference velocity, 1.4%, is the maximum of the average of the bottom two layers of the compressional velocity model HMSL – P06 [*Houser et al.*, 2007] scaled by the conversion factor of 75%. The thin solid lines in Figure 8A and 8C represent the mapping of shear and compressional velocity anomalies to temperature assuming that their respective fastest anomalies in

the lowermost mantle are due to temperature variations alone. In the case where V_P increases with the post-perovskite phase change, it and the temperature effect combine to produce a larger decrease in velocity as temperature increases than in the case of temperature alone, as is also seen in the shear velocity. In the case where V_P decreases with the post-perovskite phase change, the temperature and the phase change have competing effects so there is little change in compressional velocity with increasing temperature. Again, since the post-perovskite layer is never completely annihilated, the basic effect is to change the $d \ln V_P / dT$ coefficient.

The predicted compressional velocity variations can now be compared with those observed to assess which scenario is more consistent with our current seismic observations of the lowermost mantle. Using the average of the bottom two layers of the shear velocity model HMSL – S06, the relative temperature of the region can be found using the function shown in Figure 8A. Then the temperature function in Figure 8C is used to extract the predicted compressional velocity associated with that region, creating a predicted map of $d \ln V_P$ for the lowermost mantle, shown in the top row of Plate 6. The differential patterns between the observed

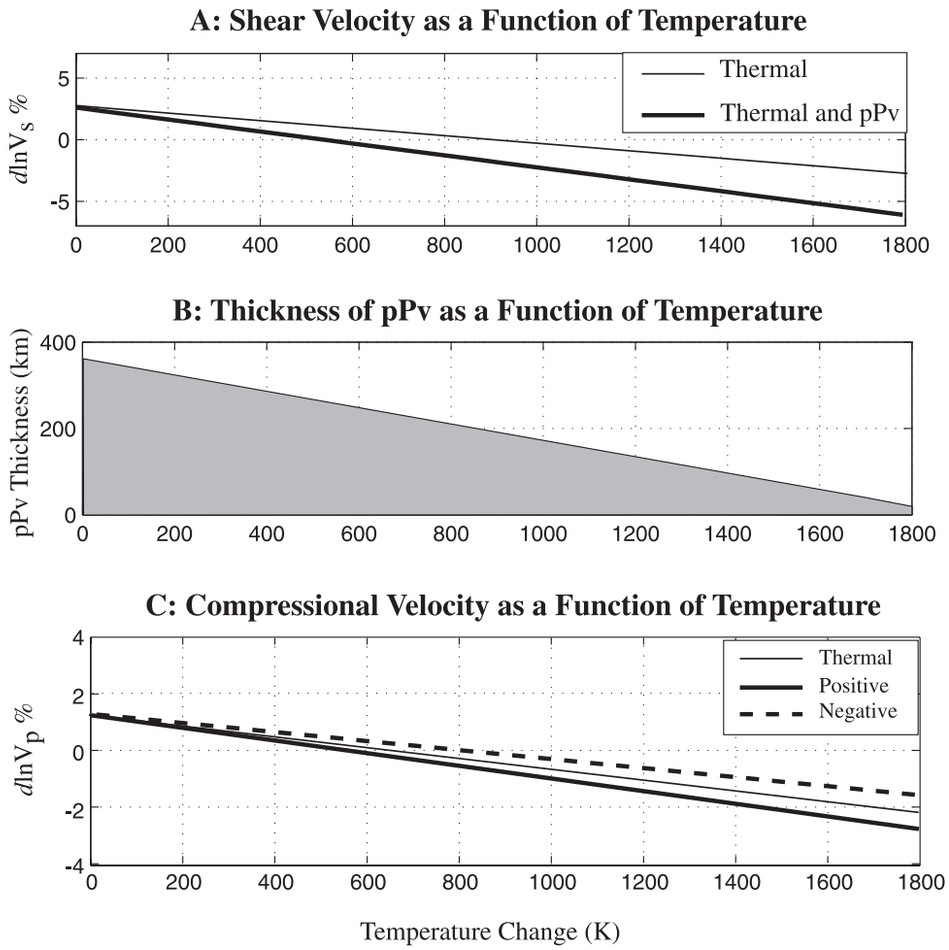

Figure 8. A: The mapping of shear velocity variations to temperature variations using the fastest region of the lowermost mantle as the starting velocity at T_0 for the case in which shear velocity depends only on temperature (think solid line) and the case where shear velocity depends on temperature and the thickness of post-perovskite predicted at that temperature. B: The thickness of post-perovskite starting at an initial thickness of 350 km as reported by *Wysession et al*. [1998] at T_0 using a Clapeyron slope of 11 MPa/K. C: The mapping of compressional velocity variations to temperature variations using the fastest region of the lowermost mantle as the starting velocity at T_0 for three scenarios. 1) V_P increases by 0.5% for the post-perovskite phase change (thick solid line), 2) V_P decreases by 0.5% for the post-perovskite phase change (thick dashed line), and 3) V_P remains unchanged as Pv transforms to pPv such that the compressional velocity depends only on temperature (thin solid line). The thickness of post-perovskite shown in 13B is used to determine the post-perovskite contribution to the shear and compressional velocities.

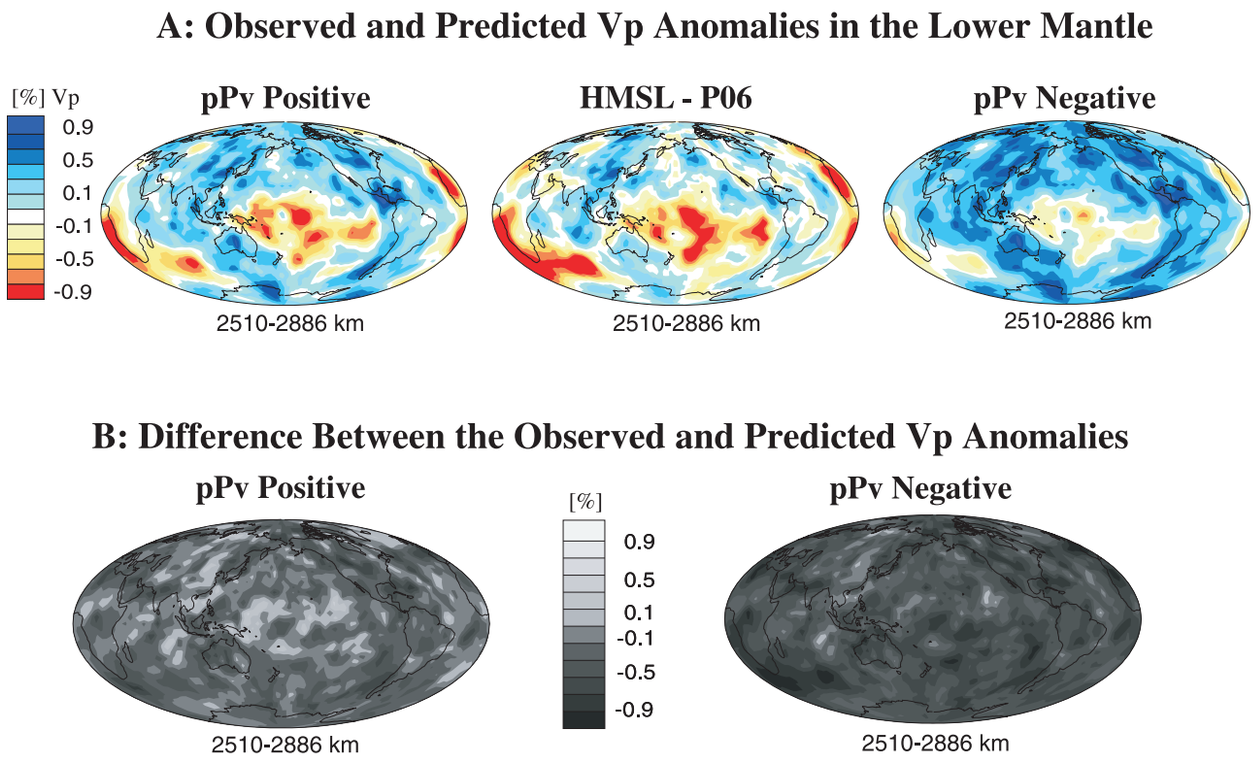

Plate 6. A: Left, the predicted compressional velocity anomalies from the scenario where the predicted velocity models in which the V_P change from Pv to pPv is positive (corresponding to the thick solid line of Figure 8C). Middle, the average of the bottom two layers of the compressional velocity model, HMSL – P06 [*Houser et al*., 2007]. Right, the predicted compressional velocity anomalies from the scenario where the predicted velocity models in which the V_P change from Pv to pPv is negative (corresponding to the thick dashed line of Figure 8C). Note, for the negative case, the shallow slope in Figure 8C causes the predicted velocities to be noticeably higher than those observed. B: The difference in the observed compressional velocity model, HMSL – P06, and the predicted velocity models in which the V_P change from Pv to pPv is positive (left) or negative (right). The predicted models are computed by taking the average of the bottom two layers of the observed shear velocity model, HMSL – S06, converting to temperature using the function in Figure 8A, and then using the functions in Figure 8C to convert temperature to compressional model variations. The mean of the observed shear and compressional models is removed since the baselines are arbitrary.

compressional model, HMSL – P06, and predicted models for the cases where the V_P increase is positive or negative for the Pv to pPv transition are shown in the bottom row of Plate 6. A grey scale is used since the baselines are uncertain in these calculations. There is less difference between the observed and predicted for the case where V_P increases with the phase transition. However, a pattern emerges in that the slow LLSVP regions are predicted to have lower velocities than observed and the circum Pacific anomalies are predicted to have higher velocities than observed. This indicates that none of these scenarios represents the reality of the lowermost mantle and that an inflection in the slope of the shear and/or compressional velocities with temperature, most likely due to composition, is still necessary to explain the observed patterns in tomography.

The slope of the velocity versus temperature curves is controlled only by our choice of $d \ln V_S / dT$ and $d \ln V_P / dT$. If the variations in shear and compressional velocities are both due only to temperature variations, then there will be no anomalous behavior in their relative variations to produce an anti-correlation of shear velocity and bulk sound speed. However, if their variations with temperature have very different slopes due to differences in their response to the post-perovskite phase change, then anomalous behavior of their relative variations should be observed. However, it is shown here that including the post-perovskite phase transition, even accounting for the uncertainty of the sign of the V_P change, cannot explain the observed relative behaviors of shear and compressional velocity in the lowermost mantle. Thus, a chemical contribution to the velocities in the lowermost mantle is still necessary to produce the relative behavior of shear and compressional velocities despite the presence of post-perovskite.

6. CONCLUSION

The current theoretical results suggest that the post-perovskite phase has a 2% increase in shear velocity and density compared to perovskite [*Tsuchiya et al.,* 2004a,b; *Oganov and Ono,* 2004], which is well within the detection threshold of long-period seismic data. Therefore, this study systematically investigates the constraints that long-period seismology places on existence of post-perovskite in the lowermost mantle.

One possibility is that post-perovskite is present as a global feature in the lowermost mantle. Normal modes provide tight constraints on the radial profile of velocity and density within the Earth. Models of the 1D structure of the Earth such as PREM which are based in part on normal mode measurements indicate that the velocities and density near the base of the mantle are lower than those expected from adiabatic increases in temperature and pressure. However, within 200 km of the CMB, the sensitivity of normal modes to shear velocity and density decreases such that the high velocity post-perovskite phase could be present but not detected.

If a global increase in seismic velocity indeed existed within 200 km of the CMB due to the presence of post-perovskite, fast travel times would be a ubiquitous feature of long-period *S* wave arrivals. Thus, the pattern in the *S* wave travel times are examined in areas near the CMB that are sampled by a high density of turning rays. A shift toward faster times representing a velocity jump is found not only in tomographically fast regions beneath Alaska, Northern Eurasia, and the Cocos Plate, but also in tomographically slow regions such as the central Pacific. There are, however, many more observations in which no systematic shift in velocity is observed than there are observations of fast or slow trends in the travel-time curves. Therefore, post-perovskite appears not to be present as a global feature below 2680 km. The fast shifts in the travel-time curves consistently occur at approximately 100 km above the CMB and can be attributed to shear velocity increases on the order of 2%. Although the temperature rise at the CMB would likely cause pPv to revert back to Pv, a "double-crossing" [*Hernlund et al.,* 2005] of the phase boundary is beyond the resolution of this long-period study. The presence of relatively fast material in the predominantly slow regions of the lowermost mantle may reflect local chemical anomalies that are favorable for the Pv to pPv transition. Thus, the long-period travel-times indicate the presence of fast material consistent with post-perovskite in a variety of localized regions of lowermost 100 km of the mantle.

This study also maps the predicted lateral variations of post-perovskite based on a variety of geotherms and depths of the Pv to pPv transition for both temperature and iron dominated thermo-chemical models. The results demonstrate that the circum-Pacific fast anomalies near the CMB can be explained by the combination of low temperatures from subducting slabs and the subsequent transition to post-perovskite. However, this is only possible for a very narrow range of mantle geotherms and transition depths. Thus, if post-perovskite is a major contributor to these fast regions, then there exists a very tight constraint on the mantle geotherm if the transition depth is known. The studies of *Hirose et al.* [2006] and *Stackhouse et al.* [2005b] suggest that chemistry does not greatly affect the depth of the Pv to pPv transition. If true, this would indicate that the occurrence of post-perovskite is mainly due to local temperature variations. In this study, the temperature model controls the predicted locations of post-perovskite since the lateral iron variations are not large enough to greatly affect the depth of the Pv to pPv transition. An increase in shear velocity consistent with the Pv to pPv transition occurs in the travel-time curves at approximately 100 km above the CMB, and if the pressure of

the transition is accurate, is thus inconsistent with a significantly superadiabatic mantle geotherm, due to the shallow transition depth required to obtain lateral variations in post-perovskite (Figures 5-7). If the Clapeyron slope is known, then the geotherm can be pinpointed once the depth of the Pv to pPv transition is measured seismically. However, since there is currently no consensus as to the exact depth or slope of the Pv to pPv transition, the tomographically derived thermo-chemical models provide a means to narrow the range of possibilities. The predicted occurrence of post-perovskite for both temperature models A and B suggest that the mantle geotherm lies between 2400 K and 2700 K at approximately 100 km above the CMB where the transition is observed in the travel-time curves. This result agrees with the value of 2600 K at 2700 km depth inferred by *Ono and Oganov* [2005].

Finally, tomographic models are tied to short-period observations to develop predicted shear and compressional velocity anomalies as a function of temperature change and post-perovskite thickness in the lowermost mantle. The case in which V_P increases by 0.5% with the Pv to pPv transition predicts a compressional velocity anomaly model that is most similar to the observed model. However, the amplitudes remain under-predicted, indicating that post-perovskite alone cannot explain the tomographic observation of the anti-correlation of shear velocity and bulk sound speed near the base of the mantle.

Acknowledgments. The author would like to thank Alex Hutko for helpful advice for simplifying the waveform analysis as well as Urska Manners, John Hernlund, and Quentin Williams for thoughtful reviews and discussions regarding this work. The suggestions made by an anonymous reviewer and Jeannot Trampert were greatly appreciated and made significant improvements to the manuscript. Guy Masters provided the data for Figure 2, and Peter Shearer provided the code to produce Figure 1A. The data were acquired using the IRIS Data Management Center which is funded through the Instrumentation and Facilities Program of the NSF EAR-0004370. Specific networks include, but are not limited to, GEOSCOPE, IDA, MEDNET, GEOFON, PACIFIC21, and those from the USGS. This work was made possible with funding distributed by the University of California Office of the President via the President's Postdoctoral Fellowship Program.

REFERENCES

Akber-Knutson, S., G. Steinle-Neumann, and P.D. Asimow, The effect of Al on the sharpness of the $MgSiO_3$ perovskite to post-perovskite phase transition, *Geophys. Res. Lett.*, 32, L14303, doi:10.1029/2005GL023192, 2005.

Antolik, M., Y. Gu, G. Ekstrom, and A. Dziewonski, J362D28: A new joint model of compressional and shear velocity in the Earth's mantle, *Geophys. J. Int.*, 153, 443-466, 2003.

Avants M., T. Lay, S.A. Russell, and E.J. Garnero, Shear velocity variation within the D″ region beneath the central Pacific, *J. Geophys. Res.*, 111, B05305, doi:10.1029/2004JB003270, 2006.

Backus, G., and F. Gilbert, The resolving power of gross Earth data, *Geophys. J. Roy. Astron. Soc.*, 16, 169-205, 1968.

Beghein, C., J. Resovsky, and J. Trampert, *P* and *S* tomography using normal-mode and surface waves data with a neighbourhood algorithm, *Geophys. J. Int.*, 149, 646-658, 2002.

Bolton, H., and G. Masters, Travel times of *P* and *S* from the global digital networks: implications for the relative variation of *P* and *S* in the mantle. *J. Geophys. Res.*, 106, 13,527-13,540, 2001.

Brown, J.M., and T.J. Shankland, Thermodynamic parameters in the Earth as determined from seismic profiles, *Geophys. J. R. Astron. Soc.*, 66, 579–596, 1981.

Bullen, K.E., Compressibility-pressure hypothesis and the Earth's interior, *MNRAS, Geophys. Suppl.*, 5, 355-368, 1949.

Chambers, K., and J.H. Woodhouse, Transient D″ discontinuity revealed by seismic migration, *Geophys. Res. Lett.*, 33, L17312, doi:1029/2006GL027043, 2006.

Clayton, R., and R. Comer, A tomographic analysis of mantle heterogeneities from body wave travel time data, *Trans. of the American Geophys. Union*, 64, 776, 1983.

Dziewonski, A., Mapping of the lower mantle: Determination of lateral heterogeneity in *P* velocity up to degree and order 6, *J. Geophys. Res.* 89, 5929-5952, 1984.

Dziewonski, A., B. Hager, and R. O'Connell, Large-scale heterogeneities in the lower mantle, *J. Geophys. Res.*, 82, 239-255, 1977.

Dziewonski, A., and D. Anderson, Preliminary reference Earth model, *Phys. Earth Planet. Int.*, 25, 297-356, 1981.

Dziewonski, A., and J. Woodhouse, Global images of the Earth's interior, *Science*, 236, 37-48, 1987.

Forte, A., and J. Mitrovica, Deep-mantle high-viscosity flow and thermochemical structure inferred from seismic and geodynamic data, *Nature*, 410, 1049-1055, 2001.

Giardini, D., X.-D. Li, and J.H. Woodhouse, Three-dimensional structure of the earth from splitting in free oscillation spectra, *Nature*, 325, 405-411, 1987.

Grand, S., Mantle shear structure beneath the Americas and surrounding oceans, *J. Geophys. Res.*, 99, 11,591-511,621, 1994.

Gu, Y.J., A. Dziewonski, W.-J. Su, and G. Ekström, Models of the mantle shear velocity and discontinuities in the pattern of lateral heterogeneities, *J. Geophys. Res*, 106, 11169-11199, 2001.

Hager, B., R. Clayton, M. Richards, R. Comer, and A. Dziewonski, Lower mantle heterogeneity, dynamic topography and the geoid, *Nature*, 313, 541-545, 1985.

He, X., and J. Tromp, Normal-mode constraints on the structure of the Earth, *J. Geophys. Res.*, 101, 20,053-20,082, 1996.

Helmberger, D., T. Lay, S. Ni, and M. Gurnis, Deep mantle structure and the postperovskite phase transition, *Proc. Natl. Acad. Sci. U. S. A.*, 102, 17,257-17,263, 2005.

Hernlund, J., C. Thomas, and P. Tackley, A doubling of the post-perovskite phase boundary and structure of the Earth's lowermost mantle, *Nature* 434, 882-886, 2005.

Hernlund, J., S. Labrosse, Geophysically consistent values of the perovskite to post-perovskite transition Clapeyron slope, *Geophys. Res. Lett.*, 34, L05309, doi: 10.1029/2006GL028961, 2007.

Hirose, K., N. Takafuji, N. Sata, and Y. Ohishi, Phase transition and density of subducted MORB crust in the lower mantle. *Earth Planet. Sci. Lett.*, 237, 239-251, 2005.

Hirose, K., Postperovskite phase transition and its geophysical implications, *Rev. Geophys.*, 44, doi: 10.1029/2005RG000186, 2006.

Hirose K., R. Sinmyo, N. Sata, and Y. Ohishi, Determination of post-perovskite phase transition boundary in $MgSiO_3$ using Au and MgO pressure standards, *Geophys. Res. Lett.*, 33, L01310, doi:10.1029/2005GL024468, 2006.

Holmes, A., J. Moriarty, G. Gathers, and W. Nellis, The equation of state of platinum to 660 GPa (6.6 Mbar), *J. Appl. Phys.*, 66, 2962-2967, 1989.

Hutko, A.R., T. Lay, E.J. Garnero, and J. Revenaugh, Seismic detection of folded subducted lithosphere at the core-mantle boundary, *Nature*, 441, 333-336, 2006.

Ishii, M., and J. Tromp, Even-degree lateral variations in the Earth's mantle constrained by free oscillations and the free-air gravity anomaly, *Geophys. J. Int.*, 145, 77-96, 2001.

Ishii, M., and J. Tromp, Constraining large-scale mantle heterogeneity using mantle and inner-core sensitive normal modes, *Phys. Earth Planet. Int.*, 146, 113-124, 2004.

Jackson, I., Elasticity, composition, and temperature of the Earth's lower mantle: a reappraisal, *Geophy. J. Int.*, 134, 291-311, 1998.

Jamieson, J.C., J.N. Fritz, and M.H. Manghnani, Pressure measurement at high temperature in X-ray diffraction studies: Gold as a primary standard, in *High Pressure Research in Geophysics*, edited by S. Akimoto and M.H. Manghnani, pp. 27-48, Springer, New York, 1982.

Lay, T., and D.V. Helmberger, The shear-wave velocity gradient at the base of the mantle, *J. Geophys. Res.*, 88 (10), 8160-8170, 1983.

Lay, T., J. Hernlund, E. Garnero, and M. Thorne, A post-perovskite lens and D″ heat beneath the central Pacific, *Science*, 314, 1272-1276, 2006.

Li, B., and J. Zhang, Pressure and temperature dependence of elastic wave velocity of $MgSiO_3$ perovskite and the composition of the lower mantle, *Phys. Earth Planet. Int.*, 151, 143-154, 2005.

Li, B., Characteristics of Seismic Velocity and Density Scaling Factors and their Constraints on the Lower Mantle Heterogeneities, *in preparation*, 2007.

Li, X., and B. Romanowicz, Comparison of global waveform inversions with and without considering cross-branch modal *S. A.*, 101, 15,867–15,869, 1995.

Mao, W.L., G. Shen, V.B. Prakapenka, Y. Meng, A.J. Cambell, D. Heinz, J. Shu, R.J. Hemley, and H.K. Mao, Ferromagnesian postperovskite silicates in the D″ heat layer of the Earth, *Proc. Natl. Acad. Sci. U.* of coupled spheroidal and toroidal modes, *J. Geophys. Res.*, 88, 10,285-10,298, 2004.

Masters, G., J. Park, and F. Gilbert, Observations coupling, *Geophys. J. Int.* 121, 695-709, 1983.

Masters, G., and R. Widmer, Free Oscillations: Frequencies and Attenuations, in: Global Earth Physics, A Handbook of Physical Constants, Ed T.J. Ahrens, AGU, Washington, DC, 104-125, 1995.

Masters, G., G. Laske, H. Bolton, and A. Dziewonski, The relative behavior of shear velocity, bulk sound speed, and compressional velocity in the mantle: Implications for chemical and thermal structure, in *Earth's Deep Interior: Mineral Physics and Tomography From the Atomic to Global Scale*, edited, pp. 63-87, American Geophysical Union, 2000.

Masters, G., and D. Gubbins, On the resolution of density within the Earth, *Phys. Earth. Planet Int.*, 140, 159-167, 2003.

Mattern, E., J. Matas, Y. Ricard, and J. Bass, Lower mantle composition and temperature from mineral physics and thermodynamic modeling, *Geophys. J, Int.*, 160, 973-990, 2005.

Megnin, C., and B. Romanowicz, The three-dimensional shear velocity structure of the mantle from the inversion of body, surface and higher-mode waveforms, *Geophys. J. Int*, 143, 709-728, 2000.

Montelli, R., G. Nolet, G. Masters, F. Dahlen, and S.-H. Hung, Global *P* and *PP* traveltime tomography: rays versus waves, *Geophys. J. Int.*, 158, 637-654, 2004.

Murakami, M., K. Hirose, K. Kawamura, N. Sata, and Y. Ohishi, Post-perovskite phase transition in $MgSiO_3$, *Science*, 304, 855–858, 2004.

Murakami, M., K. Hirose, N. Sata, and Y. Ohishi, Post-perovskite phase transition and mineral chemistry in the pyrolitic lowermost mantle, *Geophys. Res. Lett.*, 32, L03304, doi:10.1029/2004GL021956, 2005.

Nakagawa, T., and P.J. Tackley, Three-dimensional structures and dynamics in the deep mantle: Effects of post-perovskite phase change and deep mantle layering. *Geophys. Res. Lett.* 33*(*12*)*, doi:10.1029/ 2006GL025719, 2006.

Oganov, A.R., and S. Ono, Theoretical and experimental evidence for a post-perovskite phase of $MgSiO_3$ in Earth's D″ layer, *Nature*, 430, 445–448, 2004.

Ono, S., and A.R. Oganov, In situ observations of phase transition between perovskite and $CaIrO_3$-type phase in $MgSiO_3$ and pyrolitic mantle composition, *Earth Planet. Sci. Lett*, 236, 914–932, 2005.

Panning, M., and B. Romanowicz, A three dimensional radially anisotropic model of shear velocity in the whole mantle, *Geophys. J. Int.*, 166, 1485, 2006.

Reif, C., G. Masters, and B. Li, Variations in Lower-Mantle Temperature and Chemistry from the Perspective of Seismic Tomography, *Eos. Trans. Am. Geophys. U.*, 86. no. 52. p. 1958, 2005.

Houser, C., G. Masters, P. Shearer, and G. Laske, Shear and compressional velocity models of the mantle from cluster analysis of long-period waveforms, in revision for *Geophys. J. Int*, 2007.

Ringwood, A., Phase transformations and differentiation in subducted lithosphere: implications for mantle dynamics, basalt petrogenesis, and crustal evolution, *Journal of Geology*, 90, 611-642, 1982.

Ritsema, J., and H. van Heijst, Constraints on the correlation of *P*- and *S*-wave velocity heterogeneity in the mantle from *P*, *PP*, *PPP*, and *PKP*ab traveltimes, *Geophys. J. Int.*, 149, 482-489, 2002.

Romanowicz, B., Global mantle tomography: Progress status in the past 10 years, *Annual Reviews of Earth and Planetary Science*, 31, 303-328, 2003.

Russell, S.A., T. Lay, and E.J. Garnero, Small-scale lateral shear velocity and anisotropy heterogeneity near the core-mantle boundary beneath the central Pacific imaged using broadband *ScS* waves, *J. Geophys. Res.*, 104, 13,183–13,199, 1999.

Sengupta, M., and M. Toksoz, Three dimensional model of seismic velocity variation in the Earth's mantle, *Geophys. Res. Lett.*, 3, 84-86, 1976.

Sidorin, I., M. Gurnis, and D.V. Helmberger, Dynamics of a phase change at the base of the mantle consistent with seismological observations, *J. Geophys. Res.*, 104, 15,005–15,023, 1999.

Simmons, N., A. Forte, and S. Grand, Constraining mantle flow with seismic and geodynamic data: a joint approach, *Earth Planet. Sci. Lett.*, 246, 109-124, 2006.

Stackhouse, S., J, Brodhold, J. Wookey, J.-M. Kendall, and G. Price, The effect of temperature on the seismic anisotropy of the perovskite and post-perovskite polymorphs of $MgSiO_3$, *Earth Planet. Sci. Lett.*, 230, 1-10, 2005a.

Stackhouse, S., J. Brodholt, and G. Price, High temperature elastic anisotropy of the perovskite and post-perovskite polymorphs of Al_2O_3, *Geophys. Res. Lett.* 32, doi: 10.1029/2005GL023163, 2005b.

Su, W., and A. Dziewonski, Predominance of long-wavelength heterogeneity in the mantle, *Nature*, 352, 121-126, 1991.

Su, W., and A. Dziewonski, Simultaneous inversion for 3D variations in shear and bulk velocity in the mantle, *Phys. Earth Planet. Inter.*, 100, 135-156, 1997.

Sun, D., T.-R.A. Song, and D. Helmberger, Complexity of D″ in the presence of slab-debris and phase change, *Geophys. Res. Lett.*, 33, L12S07, doi:10.1029/2005GL025384, 2006.

Tanimoto, T., Long-wavelength *S*-velocity structure throughout the mantle, *Geophys. J. Int.*, 100, 327-336, 1990.

Tateno, S., K. Hirose, N. Sata, and Y. Ohishi, Phase relations in $Mg_3Al_2Si_3O_{12}$ to 180 GPa: Effect of Al on post-perovskite phase transition, *Geophys. Res. Lett.*, 32, L15306, doi:10.1029/2005GL023309, 2005.

Thomas, C., J.M. Kendall, and J. Lowman, Lower-mantle seismic discontinuities and the thermal morphology of subducted slabs, *Earth Planet. Sci. Lett.*, 225, 105–113, 2004a.

Thomas, C., E.J. Garnero, and T. Lay, High-resolution image of lowermost mantle structure under the Cocos Plate, *J. Geophys. Res.*, 109, B08307, doi:10.1029/2004JB003013, 2004b.

Tsuchiya, T., First-principles prediction of the *P-V-T* equation of gold and the 660-km discontinuity in Earth's mantle, *J. Geophys. Res.*, 108(B10), 2462, doi:10.1029/2003JB002446, 2003.

Tsuchiya, T., J. Tsuchiya, K. Umemoto, and R.M. Wentzcovitch, Phase transition in $MgSiO_3$ perovskite in the Earth's lower mantle, *Earth Planet. Sci. Lett.*, 224, 241-248, 2004a.

Tsuchiya, T., J. Tsuchiya, K. Umemoto, and R.M. Wentzcovitch, Elasticity of post-perovskite MgSiO3, *Geophys. Res. Lett.*, 31, doi:10.1029/ 2004GL020278, 2004b.

Trampert, J., P. Vacher, and N. Vlaar, Sensitivities of seismic velocities to temperature, pressure and composition in the lower mantle, *Phys. Earth Planet. Int.*, 124, 255-267, 2001.

Trampert, J., F. Deschamps, J. Resovsky, and D. Yuen, Probabilistic tomography maps chemical heterogeneities throughout the lower mantle, *Science*, 306, 853-856, 2004.

van der Hilst, R., M.V. de Hoop, P. Wang, S.-H. Shim, P. Ma, and L. Tenorio, Seismostratigraphy and the thermal structure of the Earth's core-mantle boundary region, *Science*, 315, 813-816, 2007.

Wentzcovitch, R.M., T. Tsuchiya, and J. Tsuchiya, $MgSiO_3$ postperovskite at D″ conditions. *Proc . Nat. Acad. Sci. USA* 103, 543-546, 2006.

Williams, Q., The temperature contrast across D″, in *The Core-Mantle Boundary Region*, edited by M. Gurnis *et al*., pp. 73–81, AGU, Washington, D. C., 1998.

Woodhouse, J., The coupling and attenuation of nearly resonant multiplets in the earth's free oscillation spectrum, *Geophys*. *J. R. Astron*. *Soc*., 61, 261-283, 1980.

Woodhouse, J., and A. Dziewonski, Mapping of the upper mantle: three-dimensional modeling of earth structure by inversion of seismic waveforms, *J. Geophys*. *Res*., 89, 5953-5986, 1984.

Woodward, R., and G. Masters, Global upper mantle structure from long-period differential travel times, *J. Geophys*. *Res*., 96, 6351-6377, 1991a.

Woodward, R., and G. Masters, Lower mantle structure from *ScS-S* differential travel times, *Nature*, 352, 231-233, 1991b.

Wysession, M.E., T. Lay, J. Revenaugh, Q. Williams, E.J. Garnero, R. Jeanloz, and L.H. Kellogg, The D″ discontinuity and its implications, in *The Core-Mantle Boundary Region*, edited by M. Gurnis *et al*., pp. 273–297, AGU, Washington, D. C, 1998.

Alden Query

[Q1] Please check the verso running head.